Contrib Mineral Petrol (2006) 151: 202–221
DOI 10.1007/s00410-005-0055-2

ORIGINAL PAPER

Robert J. Stern · Ed Kohut · Sherman H. Bloomer
Matthew Leybourne · Matthew Fouch · Jeff Vervoort

Subduction factory processes beneath the Guguan cross-chain, Mariana Arc: no role for sediments, are serpentinites important?

Received: 27 April 2005 / Accepted: 1 December 2005 / Published online: 10 January 2006

Abstract We need to understand chemical recycling at convergent margins and how chemical interactions between subducted slab and the overlying mantle wedge affect mantle evolution and magmagenesis. This requires distinguishing contributions from recycled individual subducted components as well as those contributed by the mantle. We do this by examining magmatic products generated at different depths above a subduction zone, in an intra-oceanic arc setting. The Guguan cross-chain in the intra-oceanic Mariana arc overlies subducted Jurassic Pacific plate lithosphere at depths of ~125–230 km and erupts mostly basalt. Basalts from rear-arc volcanoes are more primitive than those from the magmatic front, in spite of being derived by lower degrees of melting of less-depleted mantle. Rear-arc magmas also show higher temperatures and pressures of equilibration. Coexisting mineral compositions become more MORB- or OIB-like with increasing height above the subduction zone. Trace element and isotopic variations indicate that the subduction component in cross-chain lavas diminishes with increasing depth to the subduction zone, except for water contents. There is little support for the idea that melting beneath the Mariana Trough back-arc basin depleted the source region of arc magmas, but melting to form rear-arc volcanoes may have depleted the source of magmatic front volcanoes. Enrichments in rear-arc lavas were not caused by sediment melting; the data instead favor an OIB-type mantle that has been modestly affected by subduction zone fluids. Our most important conclusion is that sediment fluids or melts are not responsible for the K–h relationship and other cross-chain chemical and isotopic variations. We speculate that an increasing role for supercritical fluids released from serpentinites interacting with modestly enriched mantle might be responsible for cross-chain geochemical and isotopic variations.

Electronic Supplementary Material Supplementary material is available for this article at http://dx.doi.org/10.1007/s00410-005-0055-2 and is accessible for authorized users.

Editorial Responsibility: T. L. Grove

R. J. Stern (✉) · M. Leybourne
Department of Geosciences, University of Texas at Dallas, Box 830688, Richardson, TX 75083, USA
E-mail: rjstern@utdallas.edu
Tel.: +1-972-8832442
Fax: +1-972-8832537

E. Kohut · S. H. Bloomer
Department of Geosciences, Oregon State University, Corvallis, OR 97331, USA

M. Fouch
Department of Geological Sciences, Arizona State University, Box 871404, Tempe, AZ 85287, USA

J. Vervoort
Department of Geology, Washington State University, Pullman, WA 99164, USA

*Present address:*E. Kohut
Department of Geology, University of Delaware, Newark, DE 19716, USA

Introduction

Subduction zones are powerful physical and chemical engines where sediments, crust, and lithosphere sink and, on the way down, interact with asthenospheric mantle. This equilibrates Earth's mantle with its volatile- and incompatible-element-rich outer layers and produces magmas. Understanding this deep recycling system is a scientific challenge requiring multiple approaches. One valuable perspective comes from understanding how and why lava compositions vary with depth to the subduction zone, seismically defined as the Wadati-Benioff Zone (WBZ). In particular, studying lava compositions in cross-chains, oriented perpendicular to the strike of the arc magmatic front and parallel to the WBZ dip direction, should reveal how contributions from the subducted slab and sediments and overriding mantle contributions change with increasing WBZ depth.

From the earliest days of plate tectonics, it was known that magmas generated over deeper parts of a subduction zone contained more of a typical incompatible element (potassium) than melts generated over shallower parts of the same subduction zone (Hatherton and Dickinson 1969). Hatherton and Dickinson (1969) were undecided as to the cause of this systematic variation, suggesting that it could reflect either differing stabilities of K-bearing phases in the subducted slab (i.e., amphibole vs. phlogopite) or different ascent paths or melting processes. The 'K–h' relationship—which we now should expand to include more of the periodic table, including large ion lithophile (LIL) elements Rb and Ba and the light Rare Earth elements (LREE)—is still a robust constraint, but it remains unclear what this fundamental relationship reveals about subduction zone processes. We now know that nearly all of the major elements in most arc magmas come from partial melting of convecting asthenosphere above the subducting slab, and that LIL and other incompatible element abundances are due to distillation of subducted sediments (Plank and Langmuir 1993) or dehydrating oceanic crust (Ishikawa and Tera 1999). Two attractive endmember possibilities are that the K–h relationship indicates a greater role for sediment melting with greater WBZ depth, or that lower degrees of mantle melting occur as distance increases from the magmatic front. These simplified possibilities provide a useful frame for the themes addressed in this paper.

The significance of the K–h relationship can be most confidently explored using intra-oceanic arc (IOA) systems, those convergent margins built on oceanic lithosphere. Like most convergent margin magmas, IOA magmas are generally fractionated and so are affected by assimilation and fractionation. However, IOA assimilation involves mafic arc crust that is chemically and isotopically similar to the arc magmas that pass through it; furthermore this crust is more refractory than continental crust. Ergo, assimilation and its effects on magma compositions are minimized in IOA systems, particularly when compared to melts that transit the thicker and more reactive crust of continental magmatic arcs. Furthermore, involvement of lithosphere in IOA magmagenesis is unlikely to obscure melt compositions, because recently formed IOA lithosphere should not have the ancient isotopic heterogeneities and LIL enrichments of ancient subcontinental lithosphere. Finally, IOA cross-chains built on back-arc basin crust should show an absolute minimum of contamination because crust beneath such cross-chains changes from relatively thick (~20–30 km) along the magmatic front to quite thin behind the arc (~5–10 km).

Here we explore how subducted lithosphere and sediments interact with the overlying mantle wedge and make it melt. New petrologic, geochemical, and isotopic results are reported for a previously unstudied cross-chain in the southern part of the 3,500 km long–Izu–Bonin–Mariana (IBM) arc system (Fig. 1a, b). We use these results to examine how processes of melt generation vary with increasing depth to the subduction zone. To the best of our knowledge, this is the first such report for a cross-chain in an IOA setting associated with an actively spreading back-arc basin. (The Kasuga cross-chain to the north (Fig. 1b; Fryer et al. 1997; Stern et al. 1993) is associated with a portion of the Mariana Trough that is rifting, not spreading (Martinez et al. 1995).) Our most important conclusion is that sediment fluids or melts are not responsible for cross-chain chemical and isotopic variations but that supercritical fluids released from serpentinites and interacting with modestly enriched mantle might be.

Geologic setting

The Mariana magmatic front in this study is represented by Guguan island and a small submarine cone to the north of Guguan (N. Guguan) sampled during the 2001 Cook 7 expedition by dredge 50 (17°24.2′N, 145°51.8′E, 1,928–1,695 m). The Guguan cross-chain extends due west from Guguan and trend perpendicular to the magmatic front. Guguan and N. Guguan lie about 125 km above the WBZ (Fig. 1c), similar to the 115 ± 10 km mean depth for Mariana arc volcanoes (England et al. 2004). There are two rear-arc volcanoes in the cross-chain that we were able to sample during Cook 7: West Guguan (W. Guguan) and Guguan 2. The W. Guguan edifice lies on the western submerged flank of Guguan, about 150 km above the WBZ, and was sampled by Cook 7 D49 (17°15.2′N, 145°42.1′E, 1,890–1,708 m). The Guguan 2 edifice lies over a very steep part of the WBZ, with an estimated depth of 230 km (Fig. 1c). These depth estimates are approximate, but it is clear that Guguan and N. Guguan lie above shallower sections of the WBZ than do W. Guguan and Guguan 2. Crust outboard of the trench is Jurassic (Stern et al. 2003), the oldest subducted beneath any convergent margin today, so Mariana is the 'cold subduction zone' endmember for global subduction zones.

Cook 7 D46, 47, and 48 sampled W. Guguan. D46 (17°12.3′N, 145°35′E, 1,821–1,645 m) and D48 (17°16.5′N, 145°37.4′E, 2,248–2,160 m) recovered abundant fresh basalt. D47 (17°15.4′N, 145°33.6′E, 1,468–1,302 m) recovered a small amount of altered volcanics which were not studied. We tried but failed to sample another edifice ~25 km WNW of Guguan 2, probably due to thick Mn armoring. Locations of dredge materials discussed in this report are shown on Fig. 1d. The slowly spreading axis of the Mariana Trough back-arc basin lies about 75 km west of Guguan 2 (Fig. 1b), so Guguan 2 lies about one-third of the distance from the magmatic front to the back-arc basin spreading axis. At the latitude of the Guguan cross-chain (~17°20′N), the Mariana Trough spreads at a rate of 25–30 mm/year (Kato et al. 2003).

The history of volcanism in the Guguan cross-chain is poorly known. Guguan erupted in 1882–1884 but there are no records of any submarine eruptions. The small cone sampled by D50 appears to be young, as evidenced

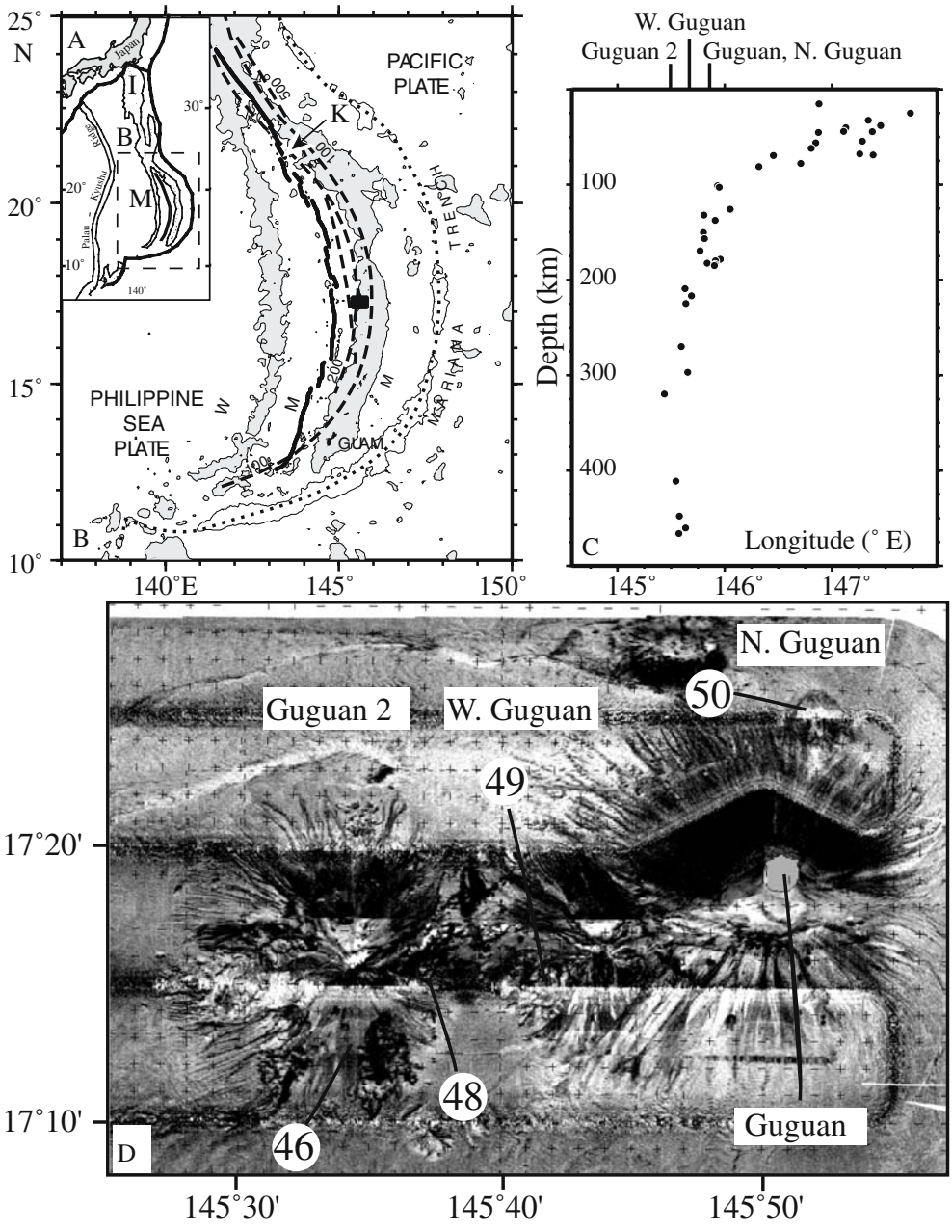

Fig. 1 **a** Locality map of the Izu (*I*)–Bonin (*B*)–Mariana (*M*) arc system. **b** Tectonic setting of the Mariana arc system (modified after Martinez and Taylor 2003). The Mariana Trough backarc basin spreading axis and rifts are shown as *heavy lines*. The Pacific Plate subducts beneath the Mariana arc at the Mariana Trench (*dotted line*), where the 6,000 m isobath is shown. The 100, 200 and 500 km contours of the Wadati-Benioff Zone (WBZ) are shown as labeled *dashed lines*. The magmatic arc (including the island of Guguan) lies about 130 km above the WBZ. Water depths shallower than 3,000 m are shown in *grey*. *Black box* shows the location of (**d**). *K* shows the location of the Kasuga cross-chain. **c** Cross-sectional view of the central Mariana subduction system using the earthquake catalog of Engdahl et al. (1998). *Black circles* denote earthquake hypocenters in a 50 km wide volume centered at 17.33°N latitude. **d** HMR-1 sonar backscatter image of the Guguan cross-chain, showing the location of dredges sampling carried out during Cook 7 expedition. Note location of Guguan island

by recovery of abundant fresh basalt with little Mn coating. W. Guguan may be extinct, as suggested by Mn-encrusted basalt recovered in D49. Guguan 2 appears to be relatively young, as suggested from good recovery of fresh basalts with little Mn coating, and by the fact that the sonar images show that debris aprons extending from the edifice onto the seafloor are not covered by hemipelagic sediments (Fig. 1d). There are no radiometric ages, but Guguan cross-chain volcanoes must have started to grow after seafloor spreading in the Mariana Trough began sometime prior to the start of the Gauss magnetic chron (2.6–3.58 Ma; Ishihara et al. 2001).

The Guguan cross-chain is a particularly interesting place to examine how elemental fluxes vary with increasing depth to the WBZ, because Guguan lavas are broadly accepted to be the magmagenetic endmember where the subduction component is delivered as hydrous fluid to the site of melt generation, with minimal contribution from subducted sediment (Elliott et al. 1997; Woodhead et al. 2001). Glass inclusions in Guguan olivines contain 2–4 wt% H_2O and average around 3 wt% H_2O (Kelley 2002). Guguan lavas show the largest ^{238}U excesses of Mariana arc lavas (Elliott et al. 1997), which is also consistent with hydrous fluxing. Guguan lavas have high $\delta^{11}B$ and high B/Nb, leading Ishikawa and Tera (1999) to conclude that most of the hydrous fluid was derived from altered oceanic crust. All of these observations are consistent with the inference that Guguan lavas represent the fluid-fluxed endmember of Mariana arc magmas (Elliott et al. 1997).

Analytical techniques

Minerals were analyzed with the Cameca SX-50 electron microprobe at Oregon State University using a 15 kV, 30 nA, 3 μm diameter beam for feldspar, and 15 kV, 50 nA, 1 μm diameter beam for olivine, pyroxene, and spinel. For feldspar and spinel analyses, count times were 10 s for all elements. Olivine analyses had count times of 20 s for Fe and Ni, and 10 s for Mg, Al, Si, K, Ti, Na, Ca, Cr, and Mn. Pyroxene analyses used count times of 20 s for Fe, Cr, and Si and 10 s for all other elements. To minimize the effects of Na migration, Na was analyzed first.

Major element concentrations were determined by Activation Laboratories using whole-rock powders. Trace element concentrations were determined at UTD by inductively compled plasma mass spectrometer (ICP-MS). Powders were prepared in an alumina ball mill. Samples (~200 mg) were weighed into teflon beakers and digested using HF, $HClO_4$, HCl, and HNO_3. Solutions were diluted 250 times in ~10% HNO_3 and further diluted 10 times in 4% HNO_3 prior to analysis. A typical analytical run of 25 samples consisted of five to six certified reference materials (CRMs), and one to two procedural blanks with the remainder being sample unknowns. CRMs included USGS standards BIR-1, W-2, BHVO-2, BCR-2, AGV-2, RGM-1, GSP-2, and G-2. Acids were distilled in-house or were purchased (Baseline grade) from Seastar Chemicals. All dilutions were prepared using 18.2 MW water from a Millipore system including an Elix reverse osmosis and electrodeionization unit and a Milli-Q Element final purification unit. Trace and rare earth elements were analyzed on a Perkin Elmer-Sciex Elan 6100 dynamic reaction cell ICP-MS (DR-ICP-MS). External calibration standards were prepared from SCP multi-element ICP standards. Samples were introduced to the ICP via an autosampler at a flow rate of 1 mL min^{-1}. Samples were nebulized using a cross-flow nebulizer and Ryton Scott spray chamber. Typical operating conditions are 0.90 L min^{-1} nebulizer gas flow, 1.30 L min^{-1} auxiliary gas flow, 13 L min^{-1} plasma gas flow at an operating RF voltage of 1,100 W. The ion lens is optimized at the start of each run and the voltage is dynamically modified by the instrument software to optimize analyte signal for masses of In. To monitor drift, a calibration standard and a CRM are run after every five unknowns. Procedural blanks are typically near or below detection for the operating conditions.

$^{87}Sr/^{86}Sr$ was determined using the Finnigan MAT 261 solid-source mass spectrometer at UTD. Reproducibility of $^{87}Sr/^{86}Sr$ is ± 0.00004. During this study, the UTD lab obtained a mean $^{87}Sr/^{86}Sr = 0.70803 \pm 3$ for several analyses of the E&A $SrCO_3$ standard; data reported here have been adjusted to correspond to a value of 0.70800 for the E&A standard. $^{143}Nd/^{144}Nd$ was also determined using the UTD Finnigan-MAT 261 in the dynamic multicollector mode. Calculations of ε_{Nd} for samples are based on values of ε_{Nd} for the UCSD standard ((15.2) and BCR ((0.16; Pier et al. 1989). A total range of ± 0.00002 observed for $^{143}Nd/^{144}Nd$ of the standard (mean value = 0.511868) is taken as the analytical uncertainty for the samples. Pb was separated using the technique of Manton (1988) and isotope ratios were also determined at UTD using the MAT 261 in the static multicollector mode and corrected for fractionation using results for the NBS-981 standard analyzed under the same conditions. Total processing blanks for Sr, Nd, and Pb are <0.1, <0.3, and <0.3 ng, respectively. Hf isotopes were analyzed by MC-ICP-MS using the ThermoFinnigan Neptune at Washington State University. Multiple analyses of the JMC 475 standard over the past year yield $^{176}Hf/^{177}Hf = 0.282146 \pm 0.000010$ (2 standard deviation (SD), $n = 63$). This number is without any bias factors applied other than the standard exponential mass bias correction. Standards within single days reproduce within a total range of about 0.000010, which is taken to approximate the analytical uncertainty. Final Hf isotopic values for samples are reported relative to $^{176}Hf/^{177}Hf = 0.282160$ for the JMC 475 Hf standard. Samples analyzed for Hf isotopes were analyzed for Lu and Hf concentrations and $^{176}Lu/^{177}Hf$ by isotope dilution using a mixed Lu–Hf tracer. The error on the $^{176}Lu/^{177}Hf$ is estimated to be 0.2%. Full details of the Lu–Hf method used at WSU, including chemistry and mass spectrometry are described in Vervoort et al. (2004).

All data for N. Guguan, W. Guguan, and Guguan 2 are new. All data for Guguan, except for EMP results, are from the literature (Elliott et al. 1997; Ishikawa and Tera 1999; Woodhead 1989; Woodhead et al. 2001).

Results

Petrography and mineral chemistry

Lavas from Guguan island have been subjected to extensive geochemical and isotopic studies but petrographically and mineralogically are relatively unstudied. These are mostly vesicular and porphyritic basalts and basaltic andesites, with abundant plagioclase phenocrysts and less abundant olivine and clinopyroxene (CPX) phenocrysts. Samples from N. Guguan (D50) have modal compositions that are similar to Guguan lavas, with 15–40% vesicles and 20–35% phenocrysts of plagioclase, CPX, and olivine (in order of decreasing abundance). Samples from W. Guguan (D49) contain 15–20% vesicles and 30–35% phenocrysts of plagioclase, clinopyroxene, and olivine. Samples from Guguan 2 are typically vesicular (1–50% vesicles) in spite of being collected from over 1,600 m deep. Guguan 2 basalts contain 1–20% phenocrysts of olivine, CPX, and plagioclase and so are less porphyritic than lavas from edifices that are closer to the magmatic front. Abundances of phenocrysts, groundmass, and vesicles are summarized in Table 1.

Phenocrysts were analyzed for representative samples for each edifice (N. Guguan: D50–1–1 and 2–1; W.

Table 1 Petrographic and major element data

	Guguan	N. Guguan			W. Guguan			Guguan 2											
	Mean mafic[a]	D50-1-1	D50-1-2	D50-1-3	D49-1-1	D49-1-2	D49-1-3	D48-1-1	D48-1-2	D48-1-3	D48-1-4	D48-2-1	D48-2-2	D48-3-1	D48-3-2	D48-3-3	D48-4-1	D46-1-2	D46-1-1	D46-1-5
Vesicles		15	30	40	35	30	20	1	50	50		15	30	20	30	35	20	40	30	25
Olivine		7	2	1	1	10	4	9	4	3		0	3	4	4.5	4	4.7	9	19	18
Plagioclase		22	24	11	10	14	21	1	1	2		1	1	0.5	0.5	0.6	0.2	0	0	1
Clinopyroxene		6	14	8	9	1	10	1	1	tr		4	1	0.5	tr	0.4	0.1	1	1	1
Groundmass		50	30	40	45	45	45	88	44	45		80	65	75	65	60	75	50	50	55
SiO_2	51.88	46.53	47.09	47.65	50.76	50.54	50.54	50.73	50.19	50.43	61.15	50.83	49.82	50.57	50.05	50.30	50.39	48.07	48.40	48.92
TiO_2	0.83	0.68	0.71	0.71	0.85	0.86	0.87	0.78	0.78	0.78	0.61	0.78	0.76	0.78	0.77	0.77	0.77	0.78	0.79	0.81
Al_2O_3	19.20	18.85	18.93	19.78	16.74	17.04	17.06	16.61	16.29	16.38	16.19	16.65	16.28	16.35	16.17	16.43	16.43	13.72	13.99	14.41
FeO*	8.98	9.51	9.43	8.77	7.87	7.91	7.92	8.32	8.26	8.32	6.51	8.23	8.19	8.32	8.24	8.29	8.30	8.28	8.25	8.24
MgO	4.06	5.81	5.84	5.51	6.91	6.86	6.84	8.23	8.56	8.61	3.11	8.16	8.13	8.66	8.63	8.16	8.28	14.26	13.68	12.80
MnO	0.19	0.15	0.17	0.16	0.15	0.15	0.15	0.16	0.16	0.16	0.15	0.16	0.16	0.16	0.16	0.16	0.16	0.16	0.16	0.15
CaO	10.56	13.17	13.43	13.87	11.96	11.93	11.95	10.77	10.70	10.80	7.21	10.80	10.58	10.77	10.71	10.71	10.71	10.43	10.47	10.65
Na_2O	2.62	1.71	1.78	1.71	2.49	2.53	2.49	2.04	2.03	2.08	2.88	2.20	2.21	2.19	2.20	2.24	2.21	1.89	1.88	1.89
K_2O	0.52	0.32	0.32	0.32	0.41	0.57	0.51	0.65	0.80	0.58	1.23	0.72	0.70	0.66	0.74	0.67	0.69	0.54	0.48	0.61
P_2O_5	0.10	0.08	0.07	0.06	0.12	0.12	0.12	0.16	0.16	0.16	0.10	0.16	0.17	0.16	0.16	0.16	0.16	0.15	0.14	0.14
Total	99.03	96.81	97.77	98.54	98.26	98.51	98.45	98.45	97.93	98.30	99.14	98.69	97.00	98.62	97.83	97.89	98.10	98.28	98.24	98.62
Mg#	44.5	52.1	52.5	52.8	61.0	60.7	60.6	63.8	64.9	64.9	46.0	63.9	63.9	65.0	65.1	63.7	64.0	75.4	74.7	73.5
Na6	1.95	1.64	1.72	1.54	2.80	2.83	2.78	2.81	2.92	2.98		2.95	2.95	3.11	3.11	2.99	3.00	4.75	4.54	4.24

Mg# = 100(Mg/Mg + Fe)

[a]Mean for 15 basalts and basaltic andesites, from Woodhead (1989), Elliott et al. (1997, and Ishikawa and Tera (1999)

Guguan: D49–1–2b; Guguan 2: D46–1–1 and D48–1-1). We also analyzed phenocrysts in two Guguan basalts (G-1 and G-2 collected by RJS in 1977). Complete analytical results are available as supplementary materials through this journal (Supplementary Tables s1, s2, s3, s4). Guguan olivine (OL) phenocrysts are Fe rich, Fo62 to Fo76, with rims as Fe rich as Fo49. These are in equilibrium with CPX, the cores of which have Mg# 64–76, also with more Fe-rich rims. OL and CPX coexist with plagioclase (PL) phenocrysts. PL phenocrysts have heterogeneous cores (An70 to An96). Phenocryst rims and groundmass feldspars are also heterogeneous, ranging from An56 to An73 (matrix) and An34 to An95 (rims). Spinels (SP) are Fe- and Ti-rich magnetites, with very low Cr contents ($Cr\# = 100Cr/Cr + Al \sim 0$). Compared to Guguan lavas, OL from N. Guguan (D50) lavas are more magnesian (Fo74–82) and are associated with similarly magnesian CPX (Mg# = 74–86), calcic PL (cores of An74–97), and titaniferous magnetite. Compared to magmatic front lavas, W. Guguan lavas contain more magnesian OL (Fo79–87) and CPX (Mg# = 78–89) and calcic PL (An70–93); small amounts of OPX (Mg# = 80) are also found in glomerophryric clusters.

Compared to phenocryst assemblages from along the magmatic front and from W. Guguan, Guguan 2 lavas contain more homogeneous and magnesian OL (D46–1-1: Fo 86–91; D48-1-1: Fo 80-89). Rare pyroxene phenocrysts in D48-1-1 are relatively fractionated (CPX Mg# = 79–82; OPX Mg# = 75–89). Groundmass PL in D46-1-1 is relatively sodic (An76–81), as are PL phenocryst cores in D48-1-1 (An77–90). Spinels in Guguan 2 lavas are also compositionally distinct from magmatic front spinels. Spinels from D46-1-1 have $TiO_2 < 0.65\%$ and are rich in Cr, with Cr# = 0.55–0.63 whereas spinels from D48-1-1 are chromites, with $TiO_2 < 0.75\%$ and Cr# up to 0.75.

Compositional relationships between mafic phenocrysts (represented by OL) and plagioclase are shown on Fig. 2a. Convergent margin OL–PL relations are generally distinct from those of MORB and OIB. Phenocrysts in magmatic front lavas (Guguan and N. Guguan) fall in the field defined by arc lavas, whereas those from W. Guguan and Guguan 2 plot in fields for MORB and OIB. These systematic differences may be due to the rotation of the plagioclase solvus as a result of high magmatic water fugacities of arc melts, so that more calcic plagioclase is in equilibrium with Fe-rich OL than is seen for anhydrous MORB and OIB (Wagner et al. 1995). This interpretation is consistent with the high (2–4%) water contents found in Guguan glass inclusions. The similarity of W. Guguan and Guguan 2 OL-PL relations to those observed in MORB and OIB suggests that the rear-arc magmas evolved under conditions of low magmatic water fugacity, but this conclusion is difficult to reconcile with estimates of water in glass inclusions (GI) in olivine phenocrysts, as discussed later.

Similar variations in spinel compositions are also found for the Guguan cross-chain (Fig. 2b). Guguan and N. Guguan spinels are magnetites, characteristic of arc lavas, whereas Guguan 2 spinels are similar to those of MORB (and OIB, not shown).

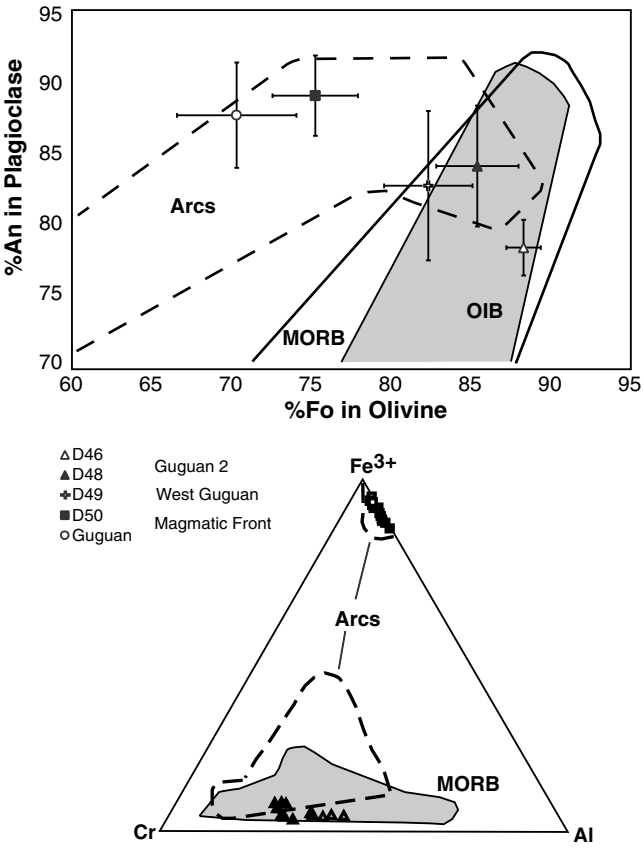

Fig. 2 **a** Plagioclase An content vs. olivine Fo for Guguan cross-chain. *Symbols* mark mean mineral pair compositions for each location and *error bars* define 2-σ variation. Note mineral pair compositions become increasing arc-like towards the magmatic front, indicating the increasing influence of water on plagioclase composition. Arc field compiled from BSVP (1981a), Conrey et al. (1997), Dixon and Batiza (1979), Meijer and Reagan (1981) and unpublished Mariana arc data. MORB field compiled from Allan et al. (1987), BSVP (1981c), Davis and Clague (1987), Niu and Batiza (1994), O'Donnell and Presnall (1980), and Perfit and Fornari (1983). OIB field compiled from Breddam (2002), BSVP (1981b, c), and Garcia et al. (2000). **b** Trivalent ion plot for spinels from Guguan cross-chain. Arc tholeiite fields (enclosed by *dashed line*) and MORB field are from Barnes and Roeder (2001). Ti-rich magnetites from D50 and Guguan lie in the arc magnetite field and D46 and D48 Cr-spinels plot in MORB field

Temperature and pressure estimates

Magmatic temperatures were estimated using the CPX-liquid geothermobarometer of Putirka et al. (1996, 2003), the olivine-liquid geothermometer of Ford et al. (1983), and the olivine-spinel geothermometers of Fabriés (1979), Roeder et al. (1979) and Balhaus et al. (1991). Olivine–spinel pairs of olivine phenocrysts with spinel inclusions were used for D46 and D48; for Guguan lavas we used the rim compositions of spinels and olivines that crystallized separately. Estimated temperatures differ between methods; the lowest are

Table 2 Estimated magmatic temperatures and pressures

	CPX-liquid T (°C)[a]		CPX-liquid P (kbar)[a]		Ol-liquid T (°C)[b]		Ol-Sp T (°C)[c]	
	Median	Range	Median	Range	Median	Range	Median	Range
Guguan	1,271	1,263–1,278	–	–	1,095	1,062–1,132	721	648–927
D50-1-1	1,237	1,228–1,244	2.2	0.8–2.7	1,091	1,076–1,105	–	–
D49–1–2	1,252	1,245–1,263	1.8	1.4–2.8	1,135	1,112–1,138	–	–
D48–1–1	1,308	1,302–1,309	6.3	6.5–6.6	1,170	1,170–1,185	1,068	1,064–1,155
D46-1-5	1,344	1,338–1,344	8.7	8.4–10.8	1,322	1,315–1,326	1,003	945–1,072

[a]Putirka et al. (1996, 2003), CPX-liquid geothermobarometer
[b]Ford et al. (1983), Ol-liquid geothermometer
[c]Fabries (1979); Roeder et al. (1979); Ballhaus et al. (1991), olivine-spinel geothermometers

from the olivine–spinel thermometers and the highest are from the CPX thermometer (Table 2). Only temperature estimates for sample D46 from the olivine-liquid and CPX-liquid thermometers are similar at ~1,322–1,344°C.

We regard the temperatures from the mineral-liquid thermometers of Ford et al. (1983) and Putirka et al. (1996, 2003) to be more reliable than the olivine–spinel temperature estimates. One issue with the latter method is that D48 olivines are oscillatory zoned. This complicates matching equilibrium olivine and spinel compositions, as the spinel inclusions we analyzed for geothermometry are located along zone boundaries. The olivine–spinel geothermometers are also pressure sensitive. Even though the two mineral-liquid thermometers mostly do not agree (except for sample D46), both show an increase in temperature away from the magmatic front and are highest for sample D46 (Table 2). However, only in sample D46 are the olivines approximately in equilibrium with bulk rock compositions, having an olivine-liquid $K_D^{(Fe/Mg)}$ of 0.29–0.3. In contrast, the CPX-liquid $K_D^{(Fe/Mg)}$ for N. Guguan at 0.27–0.29, and the Guguan lavas at 0.24–0.26 are close to the equilibrium values of 0.27 (Putrika 1999). In addition, sample D46 approaches equilibrium with a CPX-liquid $K_D^{(Fe/Mg)}$ of 0.32. Based on this characteristic, the CPX-liquid geothermometer appears to be the more reliable of the two mineral-liquid thermometers for our samples. The CPX-liquid thermometers also yield reasonable magmatic temperatures (1,228–1,344°C).

Pressures were calculated with the Putrika et al. (1996, 2003) method. Estimated pressures are from 0.8 to 3.6 kbar for D50 and D49 lavas, with median pressures of 2.2 and 1.8 kbar, respectively (Table 2). In contrast, the D48 pressures were 6.3 kbar and the D46 pressures are 8.7 kbar, revealing an increasing depth of equilibration away from the magmatic front. Unfortunately, we did not have an independent method for checking our pressure estimates, such as the Ol/CPX Ca exchange geobarometer of Köhler and Brey (1990).

Major element variations

Samples analyzed from the Guguan cross-chain are mostly basalt, with subordinate basaltic andesite and andesite (Table 1; Fig. 3a). None are Ne-normative, but normative Ol is abundant in D46 samples (12–18%) and D50 samples (2–5%). D49 and most D48 samples are Qz normative. A modest K–h relationship is observed: lavas from the magmatic front and W. Guguan straddle the low-K and medium-K fields on a potassium-silica diagram, whereas Guguan 2 samples plot in the medium-K field (Fig. 3a). Guguan and N. Guguan, lying ~ 125 km above the WBZ, together have K_{55} (K_2O contents at 55% SiO_2 by linear regression) ~0.65%, whereas Guguan 2 (~230 km above the WBZ) has K_{55}~0.9% (there is not enough spread in SiO_2 for K_{55} to be calculated in W. Guguan lavas). This agrees with an expected increase of K_{55} with increasing depth to the WBZ, but the increase is less than that predicted from the global relationship (volcanoes 125 and 230 km above the WBZ are expected to have K_{55} ~0.9 and ~2.2%, respectively Hatherton and Dickinson 1969). The values for Guguan and N. Guguan are similar to $K_{57.5}$ values of ~0.45–0.9% reported for volcanoes along the magmatic fronts of the Izu and Tonga-Kermadec arcs (Dickinson 1975). The modest increase in K with increasing WBZ depth observed for the Guguan cross-chain is similar to modest increases observed for Izu cross-chains to the north (Hochstaedter et al. 2000; Machida and Ishii 2003; Tatsumi et al. 1992). It is noteworthy that the Guguan cross-chain did not erupt shoshonites as are observed in the Kasuga cross-chain in the northern Marianas (Fryer et al. 1997).

The extent of fractionation in Guguan cross-chain lavas varies inversely with depth to the WBZ. Magmatic front lavas are strongly fractionated (Guguan basalt Mg# = 40–51; N. Guguan Mg#~53), whereas those from behind the magmatic front are primitive (melts in equilibrium with mantle peridotite) to slightly fractionated (W. Guguan Mg# = 61; Guguan 2 basalt Mg# = 63–75). This is also observed from Ni and Cr variations, which increase from < 55 ppm Ni and < 100 ppm Cr along the magmatic front to 60–80 ppm Ni and ~140 ppm Cr for W. Guguan and 100–380 ppm Ni and 260–900 ppm Cr for Guguan 2.

Variations in alkali metal contents indicate that magmatic front melts reflect higher degrees of melting than those to the rear. Na_6 (defined as Na_2O contents at 6% MgO) varies inversely with melt fraction (F) globally (Plank and Langmuir 1988). Guguan and N. Guguan lavas together define a trend indicating

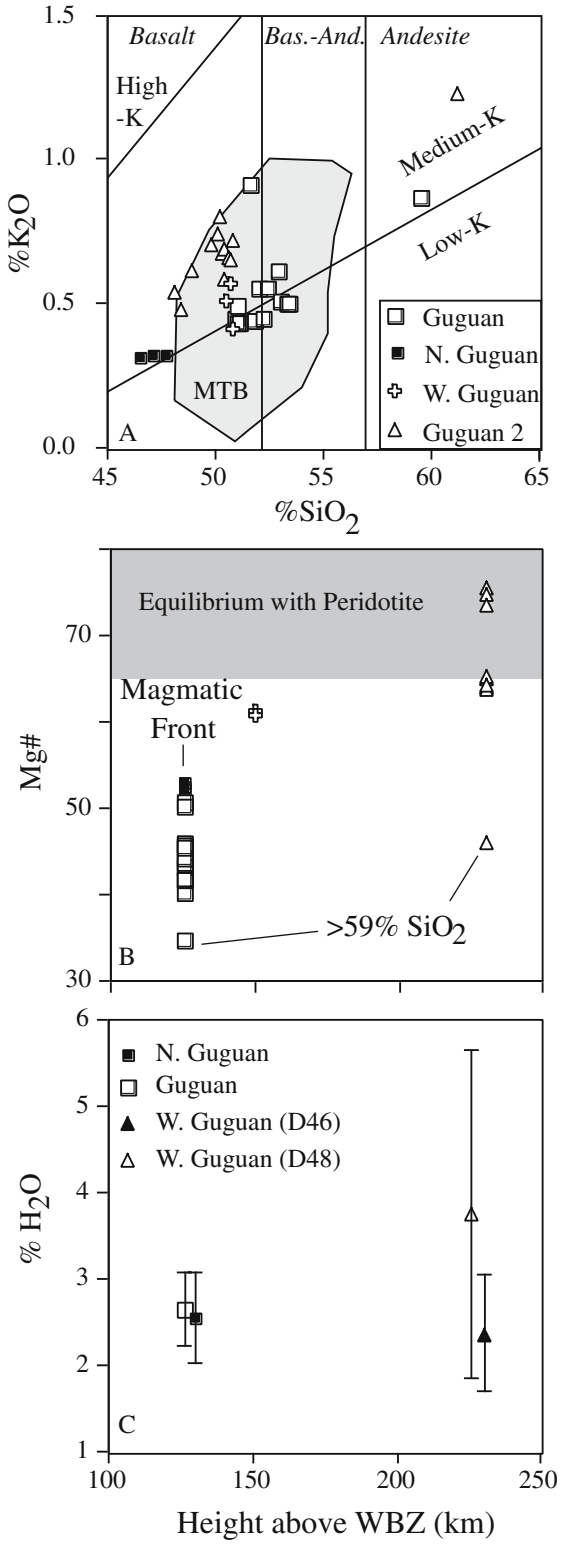

Fig. 3 **a** Potassium-silica diagram. Data for North Guguan (N. Guguan), West Guguan (W. Guguan) and Guguan 2 are from this report; data for Guguan are from Elliott et al. (1997), Ishikawa and Tera (1999), and Woodhead (1989). **b** Mg# vs. depth to WBZ. Note that lavas are more primitive (higher Mg#) with distance from the magmatic arc. Andesitic samples are noted. **c** Water contents in glass inclusions in olivines, showing mean and range for analyses (A. Shaw, written communication, 2004). There is no significant variation in water contents of cross-chain lavas

Na_6~1.9%, at the low end of the range of Na_6 for Mariana volcanoes (Maug 1.9%, Pagan 2.5% and Sarigan 2.7%; Plank and Langmuir 1988), but similar to the mean for Izu arc volcanoes ($Na_6 = 1.9 \pm 0.3\%$). Using the Na–Mg regression for Guguan and N. Guguan lavas, basalts from W. Guguan (Na_6~2.8%) and Guguan 2 (Na_6~3.3%) represent significantly lower degree melts than those from beneath the magmatic front. The covariation of alkali metals is noteworthy; the increase in Na_6 of ~70% from the magmatic front to Guguan 2 is similar to the increase in K_{55} of ~50% and suggests that these variations are due to similar controls, probably F. Note that Guguan 2 is associated with a potential melting column that is about twice as high as that beneath Guguan but erupts melts formed by a smaller extent of melting (lower F). This indicates that variations in F beneath cross-chains are not controlled by the height of the melting column, a variable which globally explains most of the differences found for F associated with the magmatic front of arcs (Plank and Langmuir 1988).

It is important to note that there is no significant variation in water contents in cross-chain lavas, as evidenced by olivine-hosted GI (Fig. 3c; A. Shaw, written communication, 2004). Olivines in one Guguan sample (GUG-3) have mean H_2O ($n = 75$) of $2.64 \pm 0.43\%$ (1 SD), similar to a mean H_2O ($n = 49$) of $2.54 \pm 0.52\%$ in olivine-hosted GI in two N. Guguan (D50) samples. This estimate of ~2.6% H_2O is within the range of 2–4 wt% H_2O in Guguan GI (Kelley 2002) and 1.4–3.3% H_2O in Mariana arc basaltic GI determined by Newman et al. (2000). Paradoxically, GI from olivines in Guguan 2 lavas are not drier than melts from the magmatic front; GI in D46 olivines have mean H_2O ($n = 19$) of $2.36 \pm 0.71\%$, whereas those from D48 have mean H_2O ($n = 6$) of $3.74 \pm 1.86\%$.

Trace element variations

Trace element variation diagrams (Table 3, Fig. 4) show that all Guguan cross-chain lavas are enriched in fluid-mobile incompatible elements (Rb, Ba, U, K, Sr, and Pb) and depleted in high field strength incompatible elements (HFSE: Nb, Zr, Ta, HREE), as is typical of convergent margin magmatic suites. Rare Earth Element (REE) abundances vary systematically along the cross-chain. Chondrite-normalized ratios $(X/Y)_n$ of REE reveal that magmatic front lavas have flat REE patterns, (mean $(La/Nd)_n$ = 0.95 for Guguan, 1.06 for N. Guguan) but become increasingly LREE-enriched (mean $(La/Nd)_n$ = 1.18 and 1.39 for W. Guguan and Guguan 2, respectively) rearword, similar to rear-arc enrichments shown by the K–h relationship. HREE patterns are also nearly flat for Guguan and N. Guguan ($(Gd/Yb)_n$ = 1.12 and 1.06, respectively), and are slightly steeper for W. Guguan ($(Gd/Yb)_n$ = 1.28) and Guguan 2 ($(Gd/Yb)_n$ = 1.30). Europium anomalies are trivial, with $Eu/Eu^* = 0.99$ and 1.02 for Guguan and N. Guguan, respectively, 0.98 for W. Guguan, and 0.97 for

Table 3 Trace element data

	Guguan	N. Guguan			W. Guguan			Guguan 2												
	Mean mafic[a]	D50–1-1	D50-1-2	D50-1-3	D49-1-1	D49-1-2	D49-1-3	D48-1-1	D48-1-2	D48-1-3	D48-1-4	D48-2-1	D48-2-2	D48-3-1	D48-3-2	D48-3-3	D48-4-1	D46-1-1	D46-1-2	D46-1-5
Mo		0.31	0.54	0.45	0.44	0.45	0.50	3.67	0.82	0.71	3.89	-0.49	0.77	0.55	0.69	1.76		0.58	3.85	3.83
Cd			0.44	0.59	0.35		0.22	0.24	0.22	0.26	0.48	0.27	0.23	0.25	0.25	0.68		0.27	0.16	0.18
In			0.06	0.05	0.05		0.05	0.06	0.06	0.06	0.05	0.06	0.05	0.06	0.05	0.05		0.05	0.05	0.05
Be			0.34	0.35	0.58		0.57	0.63	0.70	0.66	0.69	0.66	0.67	0.70	0.67	0.65		0.64	0.61	0.63
Sc		42	44	45	40	39	40	36	35	35	26	35	34	36	35	34	34	34	35	36
V	274	360	402	387	289	267	268	260	256	247	177	243	259	261	248	268	262	228	235	239
Cr	21	51	97	61	146	127	135	347	389	398	2	262	366	424	391	354	201	813	889	907
Co		27	38	38	34	32	32	37	36	36	20	36	36	37	35	37	37	48	50	49
Ni	16	22	55	44	81	54	57	126	118	118	31	107	109	119	116	147	108	334	368	373
Cu	103	55	152	89	78	81	84	64	72	62	44	66	68	65	63	75	65	62	60	61
Zn	80	60	104	93	85	63	89	78	73	77	117	73	88	93	117	85	70	69	71	74
Rb	8.5	4.1	4.00	3.60	7.10	7.30	7.80	11.60	10.50	9.70	23.00	11.40	11.20	11.50	11.00	11.40	12.3	8.00	7.20	7.80
Sr	304	344	317	320	308	317	316	406	391	392	294	406	397	395	389	400	400	290	279	302
Y	21.9	10.4	15.1	14.1	18.7	20.4	20.6	21.4	17.3	19.5	19.8	18.7	19.6	20.1	19.2	17.2	19.3	18.3	21.8	20.1
Zr	58	21	24	25	52	52	51	51	44	41	77	45	50	52	50	49	54	53	46	52
Nb	0.91		0.47	0.47	1.30	1.32	1.31	1.57	1.43	1.28	2.01	1.41	1.51	1.52	1.44	1.43	1.62	1.85	1.56	1.73
Cs	0.32	0.31	0.41	0.17	0.31	0.14	0.34	0.24	0.41	0.39	0.57	0.42	0.40	0.40	0.39	0.40	0.25	0.34	0.16	0.16
Ba	169	62	76	87	117	125	122	176	169	176	360	169	170	168	166	171	170.00	105	98	110
La	3.73		2.6	2.3	4.56	4.78	4.95	8.19	6.48	7.19	7.51	6.92	7.37	7.6	7.13	6.5	7.39	6.43	7.63	6.94
Ce	9.33		6.92	6.52	11.31	10.94	11.52	20.95	13.25	15.53	14.82	14.98	16.03	16.49	15.27	14.6	15.15	14.33	16.59	15.73
Pr	1.53		0.93	0.82	1.56	1.72	1.62	2.19	1.97	2.07	1.85	1.98	2.11	2.17	2.02	1.85	2.22	1.95	2.22	1.99
Nd	7.63		4.69	4.25	7.62	8.57	8	10.88	9.06	9.55	8.65	9.18	9.83	10.25	9.35	8.56	10.30	9.26	11.19	10.05
Sm	2.40		1.5	1.42	2.37	2.59	2.44	3.01	2.52	2.68	2.35	2.52	2.72	2.79	2.6	2.35	2.80	2.61	3.23	2.86
Eu	0.88		0.58	0.57	0.85	0.84	0.89	0.95	0.79	0.94	0.67	0.89	0.96	0.99	0.92	0.83	0.89	0.91	1.00	0.89
Gd	3.11		2.04	1.99	3.01	2.92	3.13	2.83	2.74	3.18	2.20	3.06	3.29	3.46	3.20	2.85	3.07	3.13	3.07	2.61
Tb	0.59		0.37	0.37	0.53	0.49	0.55	0.47	0.43	0.55	0.36	0.52	0.56	0.58	0.54	0.49	0.48	0.54	0.50	0.42
Dy	3.52		2.27	2.27	3.15	3.49	3.29	3.20	2.99	3.23	2.67	3	3.23	3.37	3.15	2.85	3.35	3.09	3.40	2.94
Ho	0.78		0.53	0.54	0.72	0.75	0.75	0.69	0.62	0.71	0.57	0.68	0.72	0.77	0.7	0.65	0.71	0.69	0.70	0.60
Er	2.21		1.55	1.57	2.05	2.20	2.11	1.96	1.83	2.03	1.74	1.91	2.06	2.16	2	1.87	2.09	1.93	1.99	1.76
Tm	0.35		0.22	0.23	0.3	0.32	0.3	0.28	0.26	0.29	0.24	0.28	0.29	0.31	0.28	0.28	0.29	0.28	0.28	0.23
Yb	2.24		1.49	1.58	1.91	2.08	1.96	1.89	1.71	1.93	1.80	1.83	1.88	2.02	1.85	1.86	1.97	1.81	1.82	1.61
Lu	0.36		0.24	0.206[b]	0.299[b]	0.32	0.32	0.273[b]	0.26	0.31	0.26	0.3	0.31	0.33	0.31	0.280[b]	0.30	0.250[b]	0.250[b]	0.22
Hf	1.59			0.705[b]	1.49[b]			1.38[b]								1.49[b]		1.44[b]	1.40[b]	
Pb	2.04	2.06	2.98	2.46	3.34	3.67	3.12	3.86	3.07	2.99	5.31	2.95	3.05	3.01	3.19	5.48	4.34	2.07	3.28	3.39
Th	0.40		0.55	0.41	0.57	0.5	0.58	0.85	0.77	0.69	1.09	0.74	0.93	0.96	0.89	0.98	0.85	0.68	0.58	0.59
U	0.20		0.33	0.34	0.21	0.20	0.36	0.29	0.28	0.26	0.61	0.29	0.30	0.30	0.29	0.29	0.32	0.26	0.21	0.25
K/Rb	508	647	664	738	479	479	543	465	632	496	444	524	519	476	558	488	466	498	623	649
Th/U	2.0		1.7	1.2	2.7	2.5	1.6	2.9	2.8	2.7	1.8	2.6	3.1	3.2	3.1	3.4	2.7	2.6	2.8	2.4
Zr/Nb	63.7		51.1	53.2	40.0	39.4	38.9	32.5	30.8	32.0	38.3	31.9	33.1	34.2	34.7	34.3	33.3	28.6	29.5	30.1
Ba/La	45.3		29.2	37.8	25.7	26.2	24.6	21.5	26.1	24.5	47.9	24.4	23.1	22.1	23.3	26.3	23.0	16.3	12.8	15.8

Table 3 (Contd.)

	Guguan	N. Guguan			W. Guguan			Guguan 2									
	Mean mafic[a]	D50–1-1	D50-1-2	D50-1-3	D49-1-1	D49-1-2	D49-1-3	D48-1-1	D48-1-2	D48-1-3	D48-1-4	D48-2-1	D48-2-2	D48-3-1	D48-3-2	D48-3-3	D48-4-1	D46-1-1	D46-1-2	D46-1-5
Th/Nb	0.44		1.17	0.87	0.44	0.38	0.44	0.54	0.54	0.54	0.54	0.52	0.62	0.63	0.62	0.69	0.52	0.37	0.37	0.34
La/Yb	1.7		1.74	1.46	2.39	2.30	2.53	4.34	3.79	3.73	4.17	3.78	3.92	3.76	3.85	3.49	3.75	3.55	4.20	4.30
K/Ba	25.5	42.8	35.0	30.5	29.1	37.9	34.7	30.7	39.3	27.4	28.4	35.4	34.2	32.6	37.0	32.5	33.7	37.9	45.7	46.0
Ba/Sr	0.56	0.18	0.24	0.27	0.38	0.39	0.39	0.43	0.43	0.45	1.22	0.42	0.43	0.43	0.43	0.43	0.43	0.36	0.35	0.36
Ba/Pb	83	30	25	35	35	34	39	46	55	59	68	57	56	56	52	31	39	51	30	32
Pb/Ce	0.22		0.43	0.38	0.29	0.34	0.27	0.18	0.23	0.19	0.36	0.20	0.19	0.18	0.21	0.38	0.29	0.14	0.20	0.22
Sr/Nd	39.8		67.6	75.3	40.4	37.0	39.5	37.3	43.2	41.0	34.0	44.2	40.4	38.5	41.6	46.7	38.8	31.3	24.9	30.1

[a]Data from Woodhead (1989), Elliott et al. (1997), and Ishikawa and Tera (1999)
[b]Isotope dilution (Vervoort et al. 2004, WSU)

Guguan 2. There are modestly negative Ce anomalies for Guguan (Ce/Ce*∼0.94) but not for N. Guguan (Ce/Ce* = 1.02), W. Guguan (0.98), or Guguan 2 (0.97).

Some ratios of fluid-mobile incompatible elements (such as Rb, U, Ba, Sr, and Pb) to HFSE and REE (which are generally not thought to be transported in hydrous fluids, but see different conclusions of Woodhead et al. (2001)) vary as a function of height above the WBZ, but others do not. Ba/Th and U/Th in Guguan cross-chain lavas are compared in Fig. 5 to typical ratios for MORB (Hofmann 1988) and for bulk sediments about to be subducted beneath the Marianas (Plank and Langmuir 1998). U/Th and Ba/Th inversely vary with depth to the WBZ (Fig. 5). U/Th decreases from ∼0.5 on Guguan and ∼0.7 on N. Guguan to ∼0.48 on W. Guguan and reaches mantle-like values (∼0.38) for Guguan 2 lavas (MORB U/Th ∼0.38, subducted sediment ∼0.22). Ba/Th is taken by Pearce et al. (2005) to track the subduction component carried in hydrous fluids; this decreases from very high values along the magmatic front (Guguan range: 300–700; mean = 442, although N. Guguan Ba/Th is much lower: 140–210), to lower values for W. Guguan (∼210) and Guguan 2 basalts (130–190). All of these lavas show significantly higher Ba/Th than ∼75 typical of MORB (Hofmann 1988) or sediment subducted beneath the Marianas (∼120; Plank and Langmuir 1998).

Pearce et al. (2005) argue that Ba/Ta (and Ba/Nb) is a good proxy for the total 'subuduction component' addition to the arc magma source. Ba/Nb decreases from ∼120–200 for Guguan and N. Guguan to 70–80 for W. Guguan and 50–100 for Guguan 2 basalts, still much higher than Ba/Nb ∼4 for N-MORB (Hofmann 1988) or ∼19 for sediment subducted beneath the Mariana arc (Plank and Langmuir 1998). The depth of the Nb anomaly, as measured by La/Nb (patterns with no anomaly have La/Nb ∼1.1), does not change significantly across the cross-chain, varying from 3.5 to 6.0.

These relationships indicate that the relative contribution of fluidmobile elements U and Ba decrease with increasing slab depth. Other incompatible element pairs with a fluid-mobile element (Rb, Sr, Pb) in the numerator do not show such systematic variations. This includes Sr/Nd (∼38 on Guguan and ∼73 on N. Guguan; ∼39 on W. Guguan and ∼38 on Guguan 2), Pb/Ce (∼0.23 for Guguan and ∼0.37 for N. Guguan; 0.30 for W. Guguan, 0.24 for Guguan 2), and Rb/Zr (∼0.15 for Guguan, ∼0.17 for N. Guguan, ∼0.14 for W. Guguan, ∼0.2 for Guguan 2). Ba/Zr also shows little variation across the cross-chain (∼2.9 for Guguan and ∼3.1 for N. Guguan; 2.3 for W. Guguan and ∼3 for Guguan 2). These ratios are nonetheless higher than fresh MORB (Sr/Nd∼15, Pb/Ce∼0.041, Rb/Zr∼0.012, and Ba/Zr∼0.133 (Hofmann 1988). Relative to ratios in bulk sediments about to be subducted beneath the Marianas (Sr/Nd∼7.7, Pb/Ce∼0.19, Rb/Zr∼0.35, and Ba/Zr∼3.6 (Plank and Langmuir 1998)), cross-chain lavas have much higher Sr/Nd, similar Pb/Ce and Ba/Zr and lower Rb/Zr. These variations support the conclusion that a

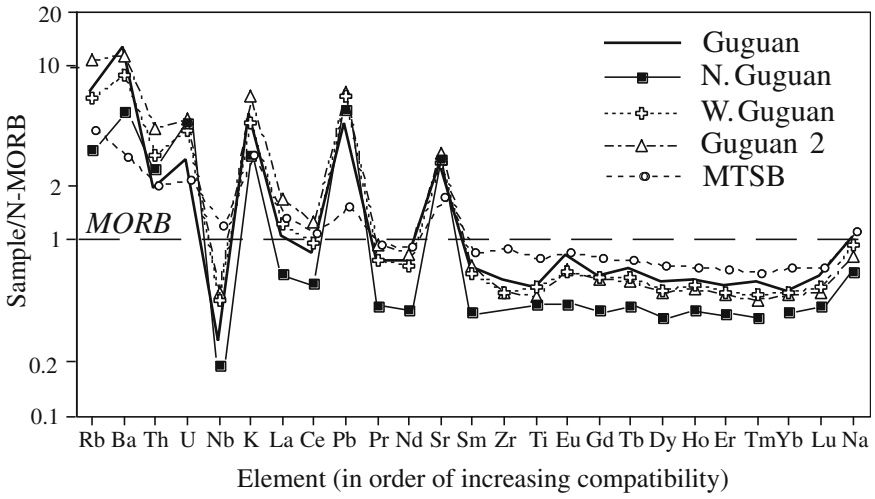

Fig. 4 Trace element variation diagram, arranged in order of elements becoming increasingly incompatible in the mantle to the left. Means for each edifice are shown. Data for Guguan are from Elliott et al. (1997), Woodhead (1989), and Woodhead et al. (2001). Element sequence and normalizing values after Hofmann (1988). *MTSB*, Mariana Trough Basalt formed by seafloor spreading

'subduction component' is carried in a hydrous fluid along the magmatic front—at least for Guguan itself—and that the contribution of this component decreases variably as WBZ increases.

Incompatible element ratios that monitor source depletion vary systematically across the Guguan cross-chain (Fig. 5). La/Yb and Zr/Y should decrease as melting proceeds, whereas Zr/Nb increases with source depletion. La/Yb increases from ~1.7 for Guguan and ~1.6 for N. Guguan (values slightly greater than La/Yb ~1.0 typical of N-MORB) to 2.4 for W. Guguan and ~3.5 for Guguan 2. Zr/Y increases slightly, from ~2.47 for Guguan and ~1.8 for N. Guguan to ~2.6 for W. Guguan and ~2.6 for Guguan 2 (MORB value ~2.9). Zr/Nb is high along the magmatic front (~60 for Guguan, ~70 for N. Guguan), decreasing rearwards (~39 for W. Guguan, ~34 for Guguan 2), approaching values for MORB (~30). Nb/Yb in melts is expected to decrease as the mantle source becomes increasingly depleted (Pearce et al. 2005). Nb/Yb is at a minimum along the magmatic front and increases from ~0.4 for Guguan and N. Guguan to ~0.8 for W. Guguan and ~1 for Guguan 2 basalts, values that approach MORB Nb/Yb ~0.92 (Hofmann 1988). These relations indicate that the mantle source of the rear-arc magmas is less depleted than that supplying the magmatic front, but cannot be due only to progressive depletion. La must be added and/or Nb subtracted from the mantle source region.

The Ba/Th vs. La/Sm diagram (Fig. 5a) was suggested by Elliott (2003) to distinguish two components responsible for much of the compositional variation observed in subduction zone magmas. The high Ba/Th, low La/Sm endmember represents melts from mantle modified by fluids from altered oceanic crust, an

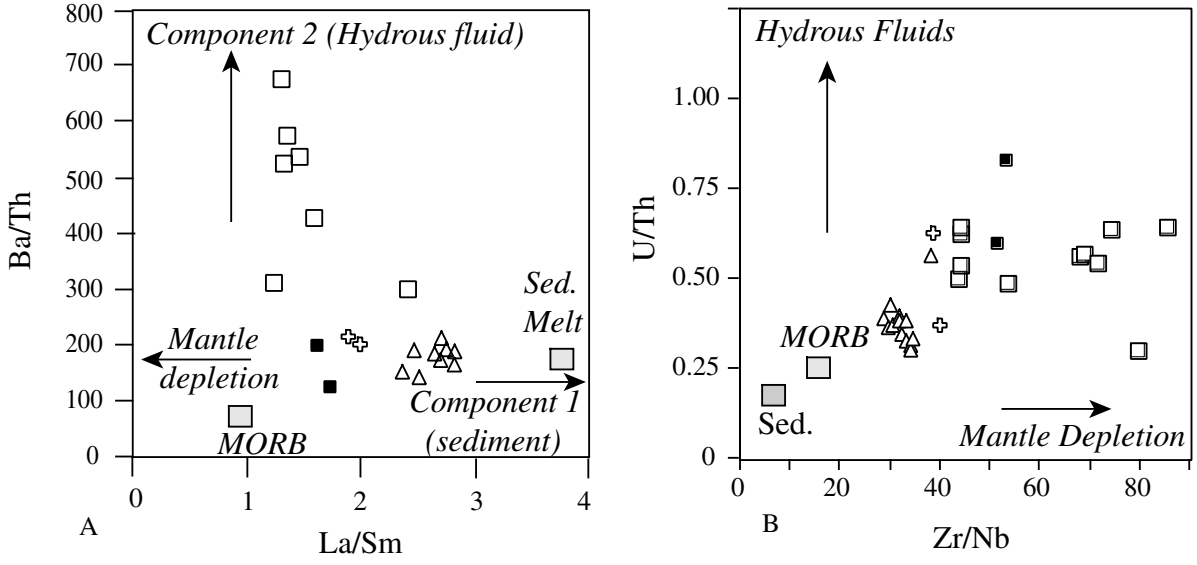

Fig. 5 Behavior of diagnostic incompatible trace elements in mafic Guguan cross-chain lavas. **a** Ba/Th vs. La/Sm, modified after Elliott (2003); **b** U/Th vs. Zr/Nb. In both cases, the element pair with the fluid-mobile element in the numerator is plotted along the *y*-axis, whereas the *x*-axis plots ratios that are sensitive to source depletion. Composition of MORB from Hofmann (1988), composition of IBM sediment melt from Hochstaedter et al. (2001)

Table 4 Isotopic data

	Guguan	N. Guguan			W. Guguan			Guguan 2												
	Mean mafic	D50-1-1	D50-1-2	D50-1-3	D49-1-1	D49-1-2	D49-1-3	D48-1-1	D48-1-2	D48-1-3	D48-1-4	D48-2-1	D48-2-2	D48-3-1	D48-3-2	D48-3-3	D48-4-1	D46-1-1	D46-1-2	D46-1-5
$^{87}Sr/^{86}Sr$	0.703469	0.703479	0.703479	0.703538	0.703202	0.703188	0.703210	0.703122	0.703115	0.703202	0.703378	0.703160	0.703166	0.703180	0.703169	0.703136	0.703152	0.703070	0.703091	0.703105
$^{143}Nd/^{144}Nd$	0.513032	0.513046	0.513078	0.512995	0.513028	0.512987	0.512997	0.512965	0.513000	0.512964	0.512956	0.513012	0.512986	0.513007	0.512975	0.512961	0.512974	0.512953	0.512942	0.512952
ε-Nd	7.80	8.18	8.79	7.18	7.82	7.03	7.21	6.59	7.27	6.57	6.42	7.50	6.99	7.42	6.79	6.52	6.77	6.35	6.14	6.33
$^{176}Hf/^{177}Hf$	0.283231[a]			0.283193	0.283229			0.283172								0.283229		0.283173	0.283171	
ε-Hf	16.3			14.9	16.2			14.1								16.2		14.2	14.1	
$^{206}Pb/^{204}Pb$	18.688	18.798	18.760	18.761	18.681	18.685	18.678	18.860	18.821	18.820	18.905	18.830	18.824	18.829	18.816	18.843	18.828	18.666	18.701	18.691
$^{207}Pb/^{204}Pb$	15.549	15.568	15.537	15.543	15.530	15.531	15.538	15.578	15.544	15.547	15.566	15.545	15.541	15.544	15.549	15.561	15.548	15.536	15.564	15.535
$^{208}Pb/^{204}Pb$	38.266	38.380	38.277	38.288	38.266	38.265	38.296	38.466	38.344	38.347	38.420	38.351	38.333	38.350	38.288	38.388	38.374	38.265	38.372	38.291
$\Delta 7/4$	3.26	3.93	1.24	1.83	1.40	1.45	2.23	4.26	1.28	1.59	2.57	1.28	0.95	1.19	1.83	2.74	1.60	2.16	4.58	1.79
$\Delta 8/4$	4.56	2.62	(3.08	(2.10	5.37	4.78	8.73	3.73	(3.76	(3.34	(6.31	(4.15	(5.22	(4.13	(8.75	(2.02	(1.61	7.08	13.55	6.66

[a]Data from Woodhead et al. (2001)

interpretation that is consistent with other lines of evidence for Guguan lavas, which plot closest to this endmember. The significance of the low Ba/Th, high La/Sm endmember is ascribed to sediment melt (Elliott 2003). This endmember could also manifest participation of enriched OIB-type mantle (Lin et al. 1989). Guguan 2 lavas approach the low Ba/Th, high La/Sm endmember. It is difficult to explain this as a manifestation of sediment melting because Th/Nb, also taken as an index of sediment melting by Elliott et al. (1997), does not vary systematically across the cross-chain. Th/Nb ranges from ~0.43 for Guguan and ~1.0 for N. Guguan to ~0.42 for W. Guguan and ~0.50 for Guguan 2. This is an order of magnitude higher than Th/Nb ~0.05 for MORB and is also significantly higher than Th/Nb ~0.24 for subducted sediment. It is similar to the value of 0.7 inferred for sediment melts beneath the northern IBM arc (Hochstaedter et al. 2001); however, the modest variations observed for the cross-chain do not indicate a more important role for sediment melts in rear-arc volcanoes relative to the role that this component plays in magmatic front melt generation.

The U/Th vs. Zr/Nb diagram (Fig. 5b) provides a different perspective on the origin of geochemical variations for the Guguan cross-chain. High U/Th is expected for mantle sources that have been metasomatized by hydrous, slab-derived fluids, whereas high Zr/Nb is expected for depleted mantle sources. Magmatic front lavas have higher U/Th and Zr/Nb than do those of rear-arc lavas, suggesting linkages between source depletion and metasomatism due to hydrous, slab-derived fluids. In contrast Guguan 2 lavas have lower U/Th and Zr/Nb and cluster near MORB, OIB (not shown on Fig. 5b), and sediment.

Isotopic variations

Isotopic compositions of Sr, Nd, Hf, and Pb (Table 4) vary with height above the WBZ. Sr and Nd vary the most, whereas Hf and Pb do not vary as systematically. $^{87}Sr/^{86}Sr$ decreases from a mean of 0.70347 for Guguan and 0.70350 for N. Guguan to 0.70320 for W. Guguan and 0.70317 for Guguan 2 (Fig. 6). We infer from the rearward decrease in $^{87}Sr/^{86}Sr$ that the mantle beneath the magmatic front is more perfused with radiogenic Sr extracted from sediments and altered oceanic crust than is the mantle farther from the trench. Nd isotopic compositions ($^{143}Nd/^{144}Nd$, reported as ε_{Nd}) also decrease across the cross-chain, from a mean of +7.8 for Guguan and +8.1 for N. Guguan to +7.4 for W. Guguan and +6.9 for Guguan 2, although scatter of ~2 epsilon units is observed for each edifice (Fig. 6).

The observed covariation of Sr–Nd isotopic compositions for Guguan cross-chain lavas is opposite to that observed for Mariana and other arc–back-arc basin magmatic pairs, for which BABB usually have higher $^{143}Nd/^{144}Nd$ and lower $^{87}Sr/^{86}Sr$ than associated arc lavas. In the case of the Marianas, ε_{Nd} increases

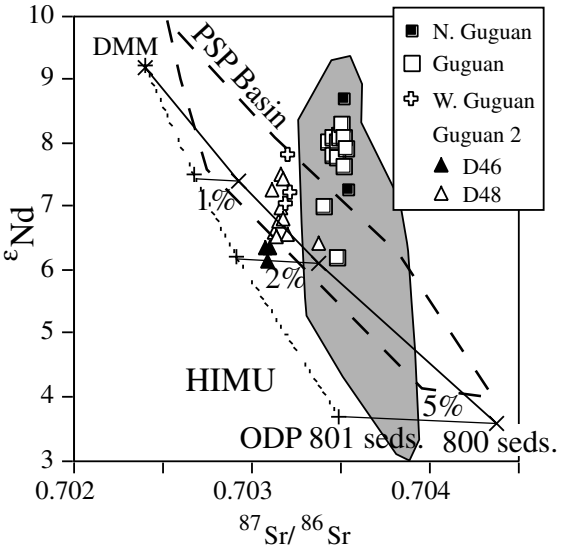

Fig. 6 Plot of Nd and Sr isotopic composition of Guguan cross-chain lavas. Cross-chain data are compared with lavas from the Mariana island arc (grey field, Stern et al. 2003) and with data for Philippine Sea Plate (*PSP*) 'basin' lavas, including samples from the W. Philippine Basin and Parece Vela-Shikoku Basin (Hickey-Vargas 1998). *Mixing curves* are shown for mixtures between depleted MORB-type mantle (*DMM*) and sediments on the subducting Pacific plate. Percent mixtures of sediment (after Plank and Langmuir 1998) are also shown. Note that the isotopic composition of Guguan 2 and W. Guguan lavas falls in the field defined by basalts from PSP basins (Hickey-Vargas 1998)

from a mean of +6.7 for lavas from the IBM magmatic front to a mean of +8.9 for Mariana Trough BABB, whereas mean $^{87}Sr/^{86}Sr$ decreases from the arc (0.70352) to Mariana Trough BABB (mean $^{87}Sr/^{86}Sr$ = 0.70291; Stern et al. 2003). The isotopic covariation seen for the Guguan cross-chain is also perpendicular to the mantle trend, where the first-order feature is the antivariation of Sr and Nd isotopic compositions. Covariation of Sr and Nd isotopic compositions is characteristic of other arc cross-chains (Hochstaedter et al. 2001; Ishizuka, et al. 2003; Stern et al. 1993; Tatsumi 2003; Woodhead et al. 1998). The antivariation of Sr and Nd isotopic compositions observed across the Kasuga cross-chain (Fig. 1b) led Stern et al. (1993) to identify a 'Frontal Arc Trend' (FAT) because lavas from the magmatic front are readily distinguished from rear-arc lavas by having higher $^{87}Sr/^{86}Sr$ at a given $^{143}Nd/^{144}Nd$, whereas rear-arc lavas define a lower $^{87}Sr/^{86}Sr$–$^{143}Nd/^{144}Nd$ 'Rear Arc Trend' (RAT). The Guguan cross-chain isotopic data also define a FAT–RAT trend that is consistent with two hypotheses. Both hypotheses accept that the FAT trend manifests addition of subducted, radiogenic Sr, largely delivered by aqueous fluids to the source of melt generation. The first hypothesis holds that the RAT trend reflects normal mantle, relatively unmodified by additions from subducted slab and sediments, whereas the second hypothesis holds that the RAT trend reflects increasing participation of sediment melts.

Pb isotopic compositions of Guguan cross-chain samples lie in the field for Mariana arc lavas (Fig. 7). Guguan lavas range in $^{206}Pb/^{204}Pb$ from ~18.5 to ~18.8, whereas data for N. Guguan (~18.75) and W. Guguan (~18.7) cluster tightly. The two dredges from Guguan 2 vary considerably, with D46 being significantly less radiogenic ($^{206}Pb/^{204}Pb$~18.7) than D48 ($^{206}Pb/^{204}Pb$~18.85). All $^{208}Pb/^{204}Pb$ data for the Guguan cross-chain plot along the Northern Hemisphere Reference Line (NHRL) and show no evidence of elevated $^{208}Pb/^{204}Pb$ characteristic of some Mariana Trough basalts as well as older lavas of the Parece Vela-Shikoku and W. Philippine Sea basins to the west (Hickey-Vargas 1998). On Pb isotope plots, Guguan cross-chain samples—like all analyses of the active Mariana arc—lie in the Pacific (as opposed to Indian ocean) field as defined by (Pearce, et al. 1999). In common with other Mariana arc lavas, Guguan cross-chain lavas have $^{207}Pb/^{204}Pb$ that is slightly to significantly displaced from NHRL towards the field for sediments. Similar observations have led others to conclude that the Pb in Guguan cross-chain lavas are derived from Pacific-type subducted sediments

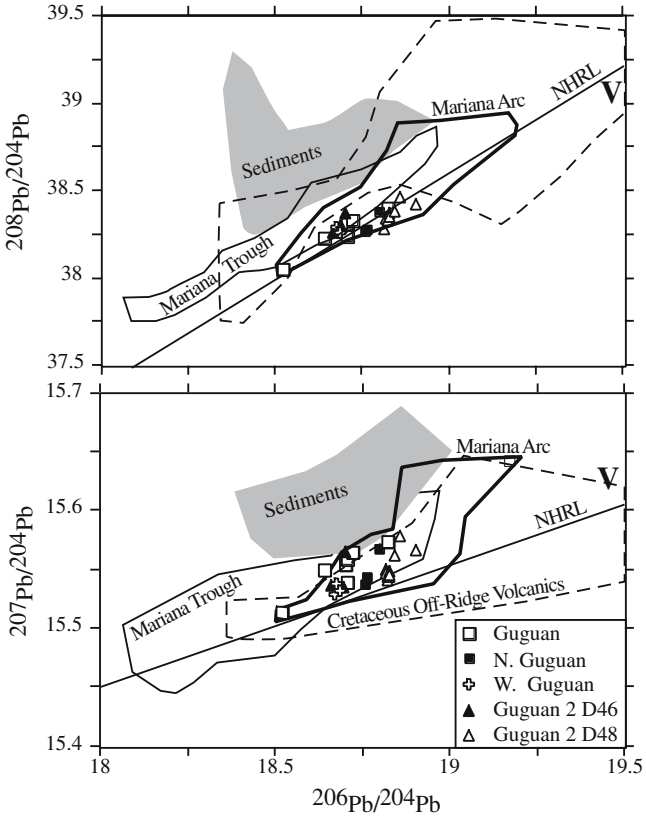

Fig. 7 Pb isotopic composition of Guguan cross-chain lavas. Fields for subducting sediments, Mariana Trough basalts, Mariana arc lavas, and Cretaceous off-ridge volcanics from Stern et al. (2003). *NHRL*, Northern Hemisphere Reference Line (Hart 1984). Fields for Mariana Trough (*thin solid line*) and Mariana arc (*thick solid line*) as well as units about to be subducted: sediments (*grey*) and Cretaceous off-ridge volcanics (*dashed line*) are from Stern et al. (2003). *Bold "V"* marks composition of OIB volcaniclastics (Elliott et al. 1997; Woodhead and Fraser 1985)

and crust (Woodhead and Fraser 1985), but it has not been explained why $^{208}Pb/^{204}Pb$ is not similarly displaced towards the field of sediments.

Seafloor subducted beneath Guguan should include volcaniclastic sediments and lava flows produced by off-ridge volcanic activity in mid-Cretaceous time. A possible explanation for the Sr–Nd RAT trend is that covariations in Sr and Nd isotopic compositions in Guguan cross-chain lavas are sourced from subducted OIB volcaniclastics and lavas, some of which have HIMU affinities. The Pb isotopic data do permit the possibility that OIB-related volcaniclastics ('V' on Fig. 7) could be important sources of Pb in Guguan cross-chain lavas. In particular, Guguan 2 D48 samples have slightly elevated $^{206}Pb/^{204}Pb$ relative to other cross-chain lavas, and this could be due to a significant contribution from HIMU volcaniclastic sediments. This possibility is inconsistent with the observation that D46 lavas plot closer to HIMU than do D48 lavas on the Sr–Nd isotopic diagram (Fig. 6).

Hf isotopic data plot in the field of Indian Ocean basalts (Fig. 8a) as defined by Pearce et al. (1999). There is relatively little variation in ε_{Hf} observed across the cross-chain (mean for Guguan = 15.9; N. Guguan = 14.9; W. Guguan = 16.2; Gugan 2 = 15.0), but the data suggest a trend that lies perpendicular to that for mixing of asthenospheric mantle and sediments (Fig. 8b).

Discussion

It is generally acknowledged that most convergent margin melts—especially those where old (> 40 Ma), cold lithosphere is subducted—are generated because the flux of hydrous fluids from the subducted slab causes mantle to melt at a much lower temperature than is normal (Gaetani and Grove 2003). Geochemical and isotopic data for Guguan cross-chain lavas, coupled with existing data for Guguan, provide a valuable perspective on several aspects of how the flux of fluids and cations from the subducted slab as well as how magma generation processes in the mantle vary with depth to the WBZ. A modest K–h relationship holds for this system, and this is because the integrated degree of melting increases towards the magmatic front. It is not clear if this reflects differences in the proportion of melting beneath each of the cross-chain volcanoes or if this is cumulative, the additive effects of sequentially melting the mantle that is advected from the rear arc towards the magmatic front. To address this question, we first examine the possible role of multiple episodes of melting resulting from the interaction of induced convection and fluxing from the subducted slab. We turn to the issue of whether or not cross-chain lava compositions indicate a progressively greater role for sediment melting with increasing depth to the WBZ.

Sequential melting as a result of induced convection

Several investigators (McCulloch and Gamble 1991; Woodhead et al. 1993) infer that the overriding asthenospheric mantle wedge is sequentially melted as it overturns beneath a convergent plate margin. In this scenario, mantle rises beneath the back-arc basin spreading ridge and migrates towards the trench before being dragged

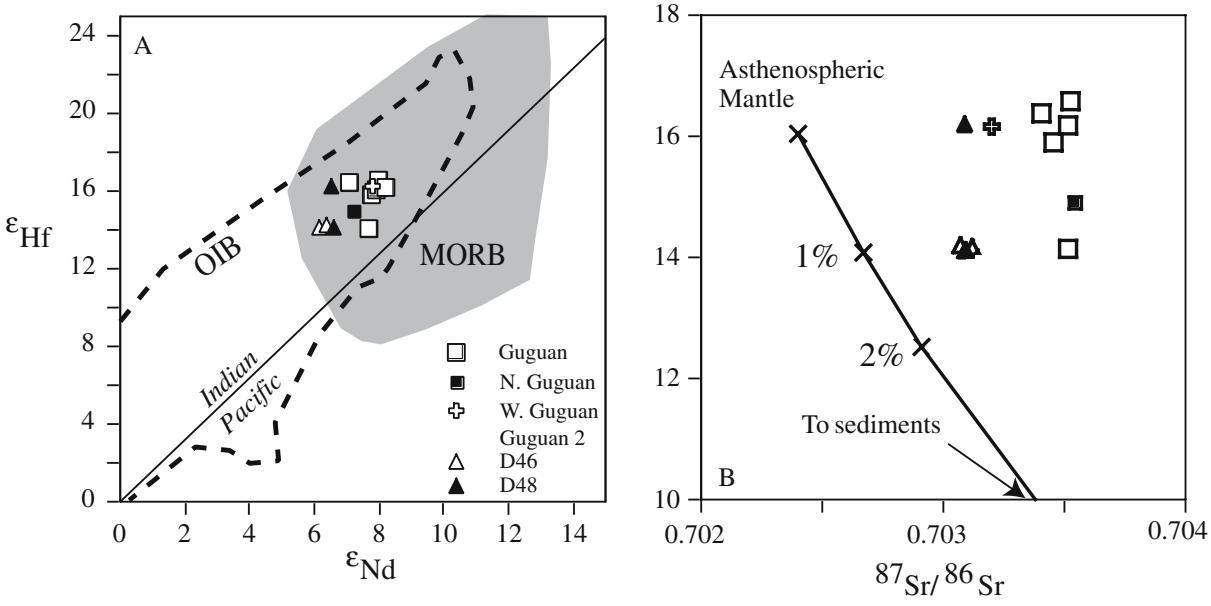

Fig. 8 **a** Hf–Nd isotopic data for Guguan cross-chain samples. *Dividing line* between Indian and Pacific mantle sources is from Pearce et al. (1999). Note that all Guguan cross-chain samples, like all Mariana arc samples, plot in the Indian Ocean mantle field. Fields for global MORB and OIB are from Vervoort et al. (1999). **b** Hf–Sr isotopic data for Guguan cross-chain samples. *Curve* shows mixing trajectory for sediment mantle mixtures, with % sediment shown. Sediment isotopic compositions are from Plank and Langmuir (1998) for Sr and J.D. Woodhead (personal communication) for Hf

down by the descending plate. Multiple opportunities for melting exist in this scenario, first pressure-release melting beneath the back-arc basin, followed by flux melting as the convecting asthenosphere approaches the magmatic arc, first beneath the cross-chains and finally beneath the magmatic front (Iwamori 1998). Melting beneath the arc may also be partly caused by decompression melting (Conder et al. 2002; England et al. 2004). Such a scenario for sequential melting beneath the Mariana Trough back-arc basin and Guguan cross-chain, modified after models of McCulloch and Gamble (1991) and Woodhead et al. (1993) is shown in Fig. 9a.

This model can be examined using simple models of batch melting. Fig. 9b and c plot ratios for 'conservative' (in the sense of Pearce and Peate 1995) incompatible elements (Nb, Yb, Zr, and Y), which are not thought to be mobile in fluids derived from the subducting slab. Figure 9b and c also shows trajectories for melting of 'primitive mantle' and the expected composition of mantle residue after 10% batch melting. For both Nb–Yb and Zr–Y systematics, Mariana Trough basalts approximate trajectories expected for batch melting of primitive mantle, although these basalts have systematically lower Nb contents than simple models predict. This is not surprising in view of the fact that BABB, like all convergent margin magmas, typically are relatively depleted in Nb relative to MORB or OIB. Ranges of ~5–15% partial melting seen on Fig. 9b and c are consistent with estimates of $13 \pm 5\%$ melting for Mariana Trough basalts that formed in association with seafloor spreading (Gribble et al. 1998).

Lavas erupted along the magmatic front of arcs characteristically show chemical signatures (Na_2O, HFSE concentrations) indicating significantly higher degrees of melting than basalts from any other tectonic environment. Arc magmas result from 10–30% melting,

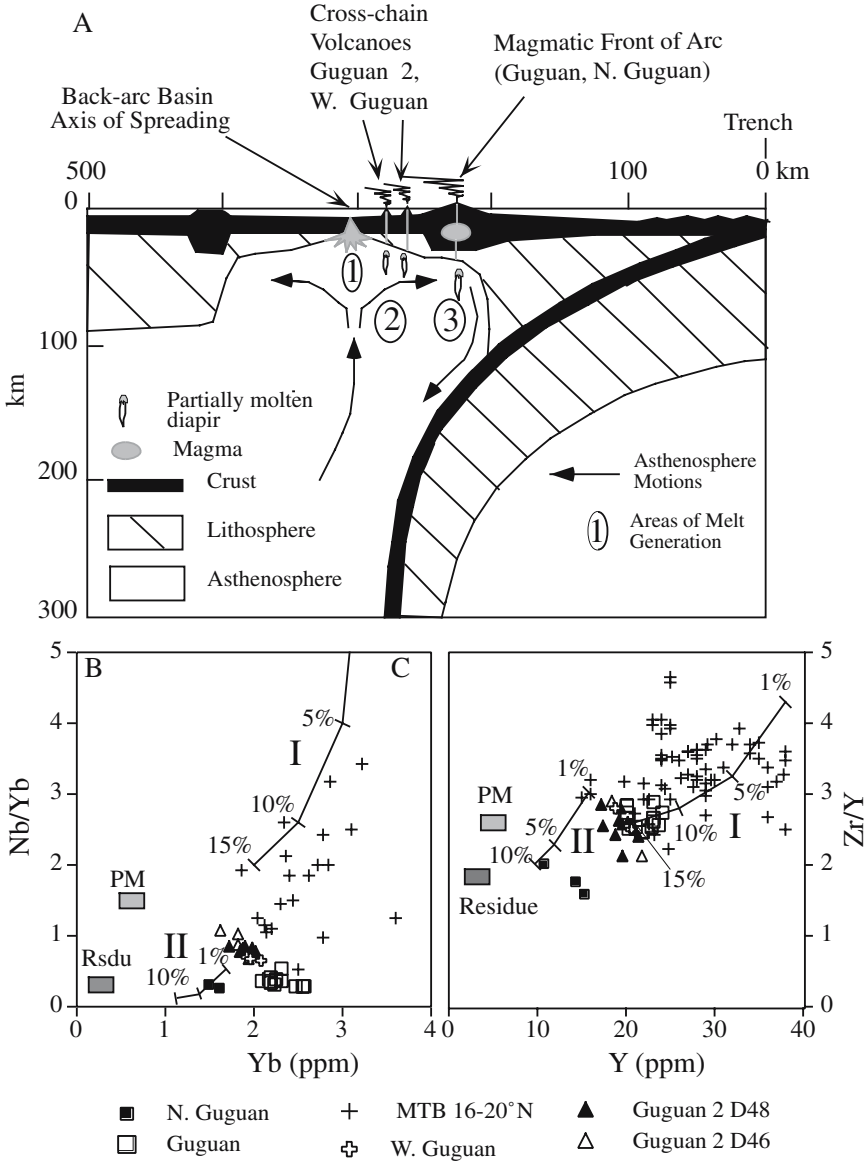

Fig. 9 Sequential melting in arc–backarc basin systems. **a** Conceptual model (no vertical exaggeration) for sequential melting beneath the Guguan cross-chain, modified after Stern et al. (2003). Note the multiple melting opportunities for convecting asthenosphere: beneath the spreading axis (*1*), beneath rear-arc cross-chain volcanoes (*2*), and beneath the magmatic front (*3*). **b** Nb/Yb vs. Yb, and **c** Zr/Y vs. Y systematics for Guguan cross-chain and Mariana Trough basalts (*MTB*); samples with $< 54\%$ SiO_2 only are plotted. Trajectories show batch nonmodal melting of spinel peridotite. Model parameters are modified after Woodhead et al. (1993). The *thin line* corresponds to batch melting of 'primitive mantle' (Hofmann 1988; *light grey box* 'PM'); the *thick line* corresponds to melting of the residue (RSD, *dark grey box*) left after 10% batch melting of primitive mantle. Data for the Mariana Trough are from Pearce et al. (2005) and other published sources

with lithospheric thickness and water content being the most important controls (Pearce and Peate 1995). The relative importance of these two factors can be assessed using variations in the extent of melting inferred for arc cross-chains. Rear-arc volcanoes are associated with a potentially much longer melting column than is the case for magmatic front volcanoes because they lie over much deeper parts of the WBZ, and in the case of the Guguan cross-chain are associated with thinner lithosphere. Nevertheless, melts from theses rear-arc volcanoes manifest lower degrees of melting, as discussed previously. Variations observed for HFS trace elements (Fig. 9b, c) are difficult to interpret as unequivocally indicating systematic differences in melting across the cross-chain. We are, nevertheless, impressed by the fact that the rear-arc lavas do not appear to be derived from a mantle source that was strongly depleted by melting beneath a back-arc basin spreading center. Guguan 2 in particular appears from trace element and isotopic perspectives to be derived from relatively undepleted mantle. This is only one cross-chain, but it is the only one that we know to be associated with an actively spreading back-arc basin in an IOA setting. The story it tells is that the mantle source of rear-arc volcanoes tap a relatively undepleted mantle source.

It appears from trace element perspectives that Guguan and N. Guguan melts were derived from a more depleted source than were those of W. Guguan and Guguan 2 (Fig. 5b). This suggests that a model of sequential melting may still be applicable to progressive depletion of cross-chain sources only, from a source that is not affected by melt depletion in the back-arc basin. A similar point has been made for Central America (Cameron et al. 2002) and Kamchatka (Hochstaedter et al. 1996) arcs. An alternate explanation is that the Guguan 2 source was depleted by melting beneath the Mariana Trough spreading ridge but has been overprinted by sediment melts so that it appears undepleted. We will show in the next section that this is not likely, because trace element and isotopic data are inconsistent with the addition of sediment melts from the subducted slab.

Another possibility is that the Guguan cross-chain represents an example of 'hot fingers' in the mantle (Tamura et al. 2002). We note that the shoalest part of the Mariana Trough back-arc basin lies about 17°N, WSW of the Guguan cross-chain (Martinez and Taylor 2003), suggesting a greater-than-normal extent of melting for this region. This part of the Mariana Trough and the Guguan cross-chain may be surficial expressions of a convecting mantle thermal anomaly. Evaluating this possibility requires shallow mantle tomographic images and thus is beyond the scope of this paper.

Was the mantle source of Guguan cross-chain magmas affected by sediment melts?

Several workers have noted the relatively enriched nature of cross-chain lavas and argued that these enrichments result from mixing sediment melt into the asthenospheric mantle source region (Hochstaedter et al. 2000; Ishizuka et al. 2003). This is an attractive explanation for the K–h relationship, because experimental results indicate that sediment melting is favored by the higher temperatures found at greater depths in the WBZ (Johnson and Plank 1999), although it should be noted that distinctions between 'fluid' and 'melt' at pressures >6 GPa (depths >180 km) do not exist (Kessel et al. 2005). Sediment melting also explains many aspects of incompatible trace element behavior for rear-arc lavas, such as Ba/La vs. La/Yb and U/Th vs. Zr/Nb (Fig. 5), where Guguan 2 lavas plot close to sediments or sediment melts. The argument for sediment melts is more difficult to reconcile with isotope data. If enrichments in Sr and Nd isotopic compositions found for rear-arc lavas are due to an increased contribution of sediments, it is reasonable to expect that these lavas should lie along an isotopic array that extends from depleted mantle towards subducted sediment. Figure 6 shows two such mixing trajectories, and Guguan cross-chain lavas trend perpendicular to both of these.

The Guguan cross-chain defines a trend that is perpendicular to that expected for mixing between MORB-type asthenospheric mantle and sediments, and this typifies global IOA cross-chain isotopic systematics. Figure 10 plots Sr and Nd isotopic compositions for several IOA cross-chains. Note that with the exception of the Kasuga cross-chain, $^{87}Sr/^{86}Sr$ generally decreases with increasing depth to the subducted slab, opposite to what would be expected if sediment melting became increasingly important with depth. Nd isotopic compositions vary less systematically as a function of depth to the subducted slab, especially considering New Britain and Kasugas, but for Guguan and the Izu cross-chains, Nd isotopic compositions also decrease with increasing WBZ depth. Thus, intra-oceanic cross-chains, considered together or individually, show little isotopic evidence for the participation of sediment melts in their source. Indeed, the W. Guguan and Guguan 2 plot in the field defined by basalts of the Philippine Sea plate, for which little subduction component has been identified (Hickey-Vargas 1998).

Pb isotopic data for Guguan cross-chain lavas are elevated towards the field for subducted sediments in $^{207}Pb/^{204}Pb$ vs. $^{206}Pb/^{204}Pb$ but not in $^{208}Pb/^{204}Pb$ vs. $^{206}Pb/^{204}Pb$, although the Pb isotopic trends do extend towards OIB volcaniclastics (Fig. 7). With the exception of more radiogenic D46 samples, there is no systematic difference between the Pb isotopic composition of lavas from the volcanic front and those from rear-arc volcanoes. In particular, cross-chain lavas do not plot closer to the field for subducted sediments than do lavas from along the magmatic front. Although not shown, it is worth noting that the elevated $^{208}Pb/^{204}Pb$ characteristic of Izu cross-chain lavas is not observed for the Guguan cross-chain. This suggests that an important isotopic province boundary lies somewhere between these beneath the IBM arc.

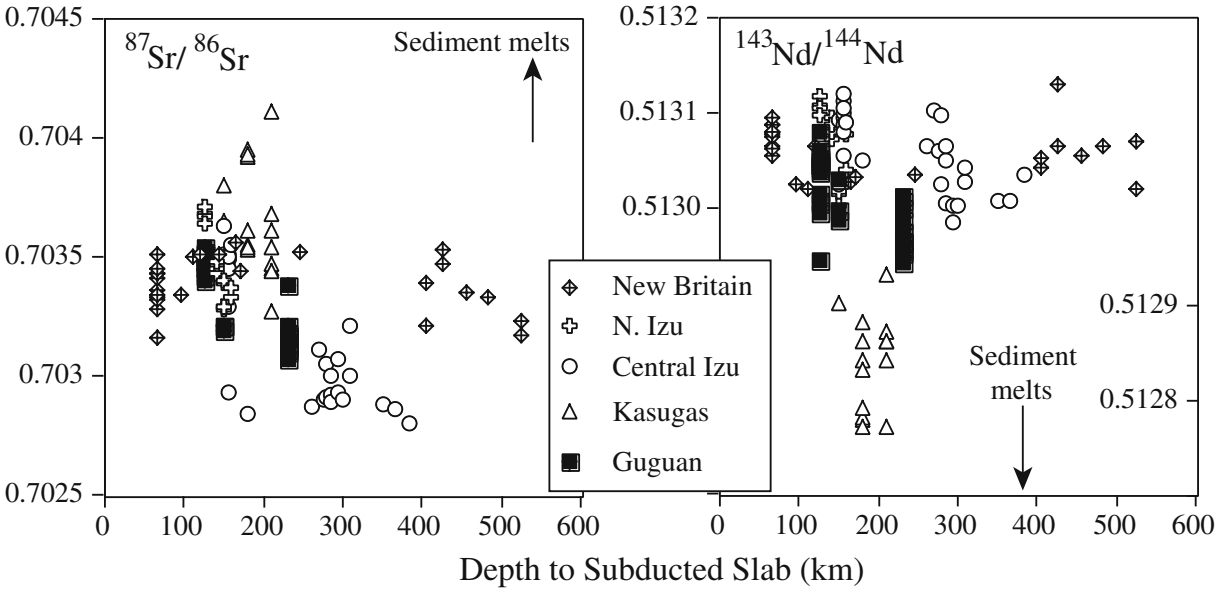

Fig. 10 **a** Plot of $^{87}Sr/^{86}Sr$ vs. height above the subducted slab; and **b** $^{143}Nd/^{144}Nd$ for five intra-oceanic cross-chains. Data for Guguan from this study, Central Izu from Hochstaedter et al. (2001) and Taylor and Nesbitt (1998), N. Izu from Taylor and Nesbitt (1998) and T. Yoshida (personal communication), Kasuga from Stern et al. (1993), New Britain from Woodhead et al. (1998) and Woodhead and Johnson (1993)

As was noted for Sr–Nd isotopic systematics, Sr–Hf isotopic variations plot along a trend perpendicular to the MORB mantle–sediment mixing trajectory. This is inconsistent with participation of sediment melts in the formation of rear-arc magmas, for the same reasons as was the case for Sr–Nd isotopic systematics.

Finally, Fig. 11 plots Th/Nb, taken as an index of sediment melt contribution (Elliott et al. 1997), versus Sr isotopic composition. Once again, the array defined by Guguan cross-chain samples is orthogonal to a mixing trajectory between MORB mantle and sediment or sediment melt. Elliott et al. (1997) argue that sediment melts in equilibrium with residual rutile could have much higher Th/Nb than the sediment itself, in which case the mixing curve could have a lower angle. Given that large variations in Th/Nb are observed for Guguan cross-chain lavas without a significant change in Sr isotopic composition, it is very difficult to endorse the idea that Th/Nb variations reflect sediment melt contributions. A similar lack of systematic variation between Th/Nb and $^{87}Sr/^{86}Sr$ led Hochstaedter et al. (2001) to disavow a role for sediment melting in controlling the K–h relationship of Izu arc cross-chains. In conclusion, we cannot find any convincing evidence that melts of subducted sediments are important for controlling the isotopic compositions of Sr, Nd, Pb, and Hf in Guguan cross-chain lavas.

Another possibility is that incompatible elements in the subducted sediments are strongly fractionated by devolatilization at shallower depths, and that melts or fluids derived from such devolatilized sediments are responsible for the enrichments observed in the cross-chain seamounts. Ryan et al. (1996) stressed that subducted slabs progressively devolatilize during descent, but also stressed the difficulty of distinguishing such fractionations due to this process versus those in the mantle. Hochstaedter et al. (2001) argued that the subduction component for rear-arc volcanoes in central Izu

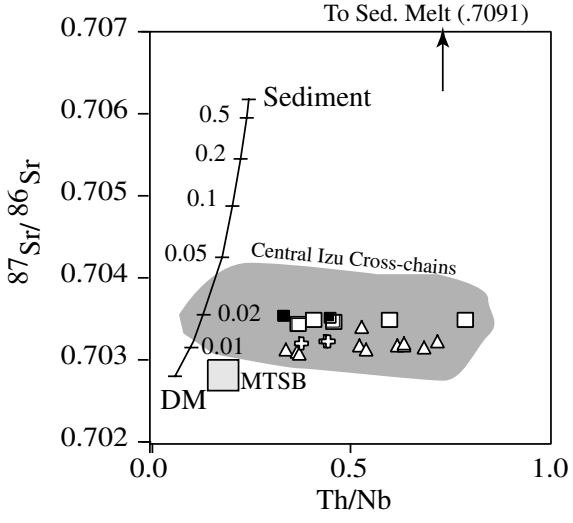

Fig. 11 Plot of $^{87}Sr/^{86}Sr$ vs. Th/Nb for Guguan cross-chain samples. *Symbols* as in Fig. 8. Mixing trajectory between asthenospheric depleted mantle (*DM*) and Western Pacific sediment (Plank and Langmuir 1998) is shown. Approximate composition of sediment melt is from Hochstaedter et al. (2001); this endmember would have higher Th/Nb and more radiogenic Sr than unmelted sediment, but data for Guguan cross-chain would still be sub-perpendicular to mixing trajectories between sediment melt and DM. *Grey field* denotes the composition of lavas from the Central Izu cross-chains (Hochstaedter et al. 2001; Taylor and Nesbitt 1998). Also shown is composition of Mariana Trough Spread basalt (*MTSB*)

cross-chain was a fluid dehydrated from a residual slab that had already been depleted in fluid-mobile elements beneath the volcanic front. In their model, the 'depleted' fluid is added to elementally and isotopically more enriched mantle beneath rear-arc volcanoes. A similar model may serve to explain the chemical composition of Guguan cross-chain lavas but not the isotopic data.

A greater role for water from Serpentinite with greater depth to the WBZ?

The variations in mineral chemical, geochemical, and isotopic compositions observed across the Guguan cross-chain are consistent with a reduced subduction component rearward. This is shown by the fact that some ratios of fluid-mobile to fluid-immobile trace elements and Sr–Nd isotopic variations in rearare lavas are distinct from magmatic front lavas and similar to OIB and MORB. These relations suggest that Guguan cross-chain rear-arc melts should be relatively anhydrous, but as Fig. 3a shows, GI in these lavas contain at least as much water as those from the magmatic front. Correcting for fractionation makes the frontal arc GI less even drier. This results in a paradox, whereby rear-arc magmas contain as much (or more) water as magmas from the magmatic front but show less trace element or isotopic evidence of a subduction component.

An intriguing possibility is that the sources of magmatic water—and the principal metasomatic agent—changes with greater WBZ depth from ones that also contain readily mobilized LIL elements, such as sediments or altered MORB, to sources that yield abundant water but little fluid-mobile large-ion lithophile elements (LILEs). Serpentinite is the best candidate, because it is extremely LIL-depleted and can carry water to greater WBZ depths than can either altered MORB or sediments (Schmidt and Poli 1998). Serpentinized mantle contains ~12% H_2O (Schmidt and Poli 1998) and this water, when released by dehydration, would carry little LILE. Faulting at the outer trench swell may allow water to seep deep into the cold lithosphere about to be subducted, serpentinizing much of the shallow mantle lithosphere (Ranero et al. 2003). In addition, sub-forearc mantle is pervasively serpentinized by fluids emanating from the downgoing slab and sediments (Peacock and Hyndman 1999), and much of this serpentinite may be entrained as part of a 'viscous blanket' developed adjacent to the downgoing slab (Kincaid and Sacks 1997). Both of these serpentinite zones may yield water upon dehydration (Yamasaki and Seno 2003). Most cold subduction zones—including the Marianas—have two parallel zones of seismicity, and the lower zone appears to manifest where serpentinite on the downgoing slab is dehydrating (Peacock 2001).

Rüpke, et al. (2004) infer from numerical models that water is continuously released from the subducting slab with the host reservoir changing with depth. They modeled the dehydration of ~120 Ma plate, and these results indicate that sediment generally dehydrates first (at depths of ~50 km), then oceanic crust (100–200 km depth), and finally serpentinized mantle (~150–250 km depth). Guguan 2 lies ~230 km above the WBZ, allowing the possibility that magmatic water for these lavas is largely produced by dehydrating serpentinite.

The Guguan cross-chain data do not allow us to confidently interpret the geochemical and isotopic variations to be due to a change in the sources of water and LILEs in subducted oceanic crust beneath Guguan to those in subducted serpentinite and enriched mantle beneath Guguan 2. Testing this hypothesis requires determining magmatic water as well as abundances and isotopic compositions of elements that should be released from dehydrating serpentinite, such as B and Cl.

Conclusions

The Guguan cross-chain is an excellent example of convergent margin magmatism where mafic melts produced from a range of depths above the WBZ can be examined without complications arising from interactions with continental crust or lithosphere. Guguan cross-chain basalts were produced at depths of 125 km beneath the magmatic front to 230 km and show systematic variations with increasing depth, including: (1) decreasing fractionation; (2) lower degrees of melting, in spite of being associated with much higher potential melting columns and similar water contents; (3) coexisting olivine—plagioclase–spinel compositions become more like those found in MORB and OIB; (5) a modest K–h relationship; (6) involvement of less-depleted mantle; (7) relative trace element abundances indicate strong gradients in some fluid-mediated subduction components, especially U/Th and Ba/La; (8) other trace-element ratios thought to monitor fluid-mediated subduction component do not decrease with increasing WBZ depth, including Sr/Nd, Rb/Zr, Ba/Zr, and Pb/Ce, nor does the magnitude of the Nb anomaly change much; (9) isotopic compositions of Sr, Nd, and Hf become less radiogenic; (10) Pb isotopic compositions do not change significantly. These results are consistent with a model of sequential melting of mantle beneath the cross-chain. The observed variations are difficult to reconcile with the hypothesis that rear-arc lavas manifest a subduction component carried in sediment melt, and are more simply explained as a result of a reduced subduction component, perhaps released by dehydrating subducted serpentinite, being added to relatively enriched mantle.

Acknowledgments The analytical assistance of Nate Miller at UTD is greatly appreciated. We thank J. Ryan and W. Leeman for their comments. We appreciate information about water contents in glass inclusions determined by Alison Shaw and Erik Hauri (DTM). We thank the two anonymous reviewers for their thoughtful criticism. This work was supported by NSF grants OCE 0001827 and OCE 0405651 to RJS and OCE-137365 and EAR-0230145 to Vervoort. This is UTD Geosciences contribution #1075.

References

Allan JF, Batiza R, Lonsdale PF (1987) Petrology and chemistry of lavas from seamounts flanking the East Pacific Rise Axis, 21°N: implications concerning the mantle source composition for both Seamount and Adjacent EPR lavas. In: Keating B, Fryer P, Batiza R (eds) Seamounts, islands, and atolls, vol 43. American Geophysical Union, Geophysical Monograph, Washington, DC, pp 255–282

Balhaus CG, Berry RF, Green DH (1991) High presure calibration of the olivine–orthopyroxene–spinel oxygen barometer, implications for the oxidation state of the upper mantle. Contrib Mineral Petrol 107:27–40

Barnes SJ, Roeder PL (2001) The range of spinel compositions in terrestrial mafic and ultramafic rocks. J Petrol 42:2279–2302

Breddam K (2002) Kistufell: primitive melt from the Iceland mantle plume. J Petrol 43:345–373

BSVP (1981a) Island arc basalts. In: BSVP (ed) Basaltic volcanism on the terrestrial planets. Pergamon Press, New York, pp 193–213

BSVP (1981b) Ocean intraplate volcanism. In: BSVP (ed) Basaltic volcanism on the terrestrial planets. Pergamon Press, New York, pp 161–192

BSVP (1981c) Ocean-floor basaltic volcanism. In: BSVP (ed) Basaltic volcanism on the terrestrial planets. Pergamon Press, New York, pp 132–160

Cameron BI, Walker JA, Carr MJ, Patino LC, Matias O, Feigenson MD (2002) Flux versus decompression melting in stratovolcanoes in southeastern Guatemala. J Volcanol Geotherm Res 119:21–50

Conder JA, Wiens DA, Morris J (2002) On the decompression melting structure at volcanic arcs and back-arc spreading centers. Geophys Res Lett 29(15):1727. DOI 1710.1029/2002GL015390

Conrey RM, Sherrod DR, Hooper PR, Swanson DA (1997) Diverse primitive magmas in the Cascade Arc, northern Oregon and southern Washington. Can Mineral 35:367–396

Davis AS, Clague DA (1987) Geochemistry, mineralogy, and petrogenesis of basalt form the Gorda Ridge. J Geophys Res 92:10476–10483

Dickinson WR (1975) Potash-depth (K-h) relations in continental margins and intra-oceanic magmatic Arcs. Geology 3:53–56

Dixon TH, Batiza R (1979) Petrology and geochemistry of recent lavas in the Northern Marianas. Contrib Mineral Petrol 70:167–181

Elliott T (2003) Tracers of the slab. In: Eiler J (ed) Inside the subduction factory, vol 138. American Geophysical Union, Geophysical Monograph, Washington DC, pp 23–45

Elliott T, Plank T, Zindler A, White W, Bourdon B (1997) Element transport from slab to volcanic front at the Mariana arc. J Geophys Res B102:14,991–915,019

Engdahl ER, van der Hilst RD, Buland R (1998) Global teleseismic earthquake relocation with improved travel times and procedures for depth determination. Bull Seismol Soc Am 88:722–743

England P, Engdahl R, Thatcher W (2004) Systematic variation in the depths of slabs beneath arc volcanoes. Geophys J Int 156:377–408

Fabriés J (1979) Spinel-olivine geothermometry in peridotites from ultramafic complexes. Contrib Mineral Petrol 69:329–336

Ford CE, Russell DG, Craven JA, Fisk MR (1983) Olivine–liquid equilibria: temperature, pressure and compositional dependance of the crystal/liquid cation partition coefficients. J Petrol 24:256–265

Fryer P, Gill JB, Jackson MC (1997) Volcanologic and tectonic evolution of the Kasuga seamounts, northern Mariana Trough: Alvin submersible investigations. J Volcanol Geotherm Res 79:277–311

Gaetani GA, Grove TL (2003) Experimental constraints on melt generation in the mantle wedge. In: Eiler J (ed) Inside the subduction factory, vol 138. American Geophysical Union, Geophysical Monograph, Washington DC, pp 107–134

Garcia MO, Pietruska AJ, Rhodes JM, Swanson K (2000) Magmatic processes during the prolonged Puu Oo eruption of Kilauea Volcano, Hawaii. J Petrol 41:967–990

Gribble RF, Stern RJ, Newman S, Bloomer SH, O'Hearn T (1998) Chemical and isotopic composition of lavas from the Northern Mariana Trough: implications for magmagenesis in back-arc basins. J Petrol 39:125–154

Hart SR (1984) A large scale isotope anomaly in the Southern Hemisphere mantle. Nature 309:753–757

Hatherton T, Dickinson WR (1969) The relationship between andesitic volcanism and seismicity in Indonesia. J Geophys Res 74(22):5301–5310

Hickey-Vargas R (1998) Origin of the Indian Ocean-type isotopic signature in basalts from Philippine Sea plate spreading centers: an assessment of local versus large-scale processes. J Geophysical Research 103(B9):20963–20979

Hochstaedter A, Gill J, Peters R, Broughton P, Holden P, Taylor B (2001) Across-arc geochemical trends in the Izu-Bonin arc: contributions from the subducting slab. Geochem, Geophys, Geosyst 2:2000GC000105

Hochstaedter AG, Gill JB, Taylor B, Ishizuka O (2000) Across-arc geochemical trends in the Izu-Bonin arc: constraints on source composition and mantle melting. J Geophys Res 105(B1):495–512

Hochstaedter AG, Kepezhinskas P, Defant M, Drummond M, Koloskov A (1996) Insights intto the volcanic arc mantle wedge from magnesian lavas from the Kamchatka arc. J Geophys Res 101(B1):697–712

Hofmann AW (1988) Chemical differentiation of the Earth: the relationship between mantle, continental crust, and oceanic crust. Earth Planet Sci Lett 90:297–314

Ishihara T, Stern RJ, Fryer P, Bloomer S, Becker NC (2001) Seafloor spreading in the Southern Mariana Trough inferred from 3-component magnetometer data. EOS 82(47):F1202

Ishikawa T, Tera F (1999) Two isotopically distinct fluid components involved in the Mariana Arc; evidence from Nb/B ratios and B, Sr, Nd, and Pb isotope systematics. Geology 27:83–86

Ishizuka O, Taylor RN, Milton JA, Nesbitt RW (2003) Fluid-mantle interaction in an intra-oceanic arc: constraints from high-precision Pb isotopes. Earth Planet Sci Lett 211:211–236

Iwamori H (1998) Transportation of H_2O and melting in subduction zones. Earth Planet Sci Lett 160:65–80

Johnson MC, Plank T (1999) Dehydration and melting experiments constrain the fate of subducted sediments. Geochem Geophys Geosyst 1:Paper number 199GC000014

Kato T, Bevan J, Matsushima T, Kotake Y, Camacho JT, Nakao S (2003) Geodetic evidence of back-arc spreading in the Mariana Trough. Geophys Res Lett 30(12). DOI 10.1029/2002GL016757, 012003

Kelley KA (2002) Subducted fluid and sediment compositions preserved in Mariana Arc melt inclusions (abstract). EOS Trans Am Geophys Union 83(47)

Kessel R, Schmidt MW, Ulmer P, Pettke T (2005) Trace element signature of subduction-zone fluids, melts and supercritical liquids at 120–180 km depth. Nature 437:724–727

Kincaid C, Sacks IS (1997) Thermal and dynamical evolution of the upper mantle in subduction zones. J Geophys Res 102(B6):12295–212315

Köhler TP, Brey GP (1990) Calcium exchange between olivine and clinopyroxene calibrated as a geothermobarometer for natural peridotites from 2 to 60 kb with applications. Geochim Cosmochim Acta 54:2375–2388

Lin PN, Stern RJ, Bloomer SH (1989) Shoshonitic volcanism in the Northern Mariana Arc. 2. Large-ion lithophile and rare earth element abundances: evidence for the source of incompatible element enrichments in intraoceanic arcs. J Geophys Res 94:4497–4514

Machida S, Ishii T (2003) Backarc volcanism along the en echelon seamounts: the Enpo seamount chain in the northern Izu-Oasawara arc. Geochem Geophys Geosyst 4(4). 9006. DOI 9010.1029/2003GC000554

Manton WI (1988) Separation of Pb from young zircons by single-bead ion exchange. Chem Geol 73:147–152
Martinez F, Fryer P, Baker NA, Yamazaki T (1995) Evolution of backarc rifting: Mariana Trough, 20°–24°N. J Geophys Res 100:3807–3827
Martinez F, Taylor B (2003) Controls on back-arc crustal accretion: insights from the Lau, Manus and Mariana basins. In: Larter RD, Leat PT (eds) Intra-oceanic subduction systems: teconic and magmatic processes, vol 219. Geological Society, Special Publications, London, pp 19–54
McCulloch MT, Gamble AJ (1991) Geochemical and geodynamical constraints on subduction zone magmatism. Earth Planet Sci Lett 102:358–374
Meijer A, Reagan M (1981) Petrology and geochemistry of the Island of Sarigan in the Mariana Arc: calc-alkaline volcanism in an oceanic setting. Contrib Mineral Petrol 77:337–354
Newman S, Stolper E, Stern RJ (2000) H_2O and CO_2 in magmas from the Mariana arc and back arc system. Geochem Geophys Geosyst 1, paper no: 1999GC000027
Niu Y, Batiza R (1994) Magmatic processes at a slow spreading ridge segment: 26°S Mid-Atlantic Ridge. J Geophys Res 99:19719–19740
O'Donnell TH, Presnall DC (1980) Chemical variations of the glass and mineral phases in basalts deredged from 25°–30°N along the Mid-Atlantic Ridge. Am J Sci 280:845–868
Peacock SM (2001) Are the lower planes of double seismic zones caused by serpentine dehydration in subduction oceanic mantle? Geology 29:299–302
Peacock SM, Hyndman RD (1999) Hydrous minerals in the mantle wedge and the maximum depth of subduction thrust earthquakes. Geophys Res Lett 26:2517–2520
Pearce JA, Kempton PD, Nowell GM, Noble SR (1999) Hf–Nd element and isotope perspective on the nature and provenance of mantle and subduction components in Western Pacific arc-basin systems. J Petrol 40:1579–1611
Pearce JA, Peate DW (1995) Tectonic implications of the composition of volcanic arc magmas. Annu Rev Earth Planet Sci 23:251–285
Pearce JA, Stern RJ, Bloomer SH, Fryer P (2005) Geochemical mapping of the Mariana arc-basin system: implications for the nature and distribution of subduction components. Geochem Geophys Geosyst 6(7). DOI 10.1029/2004GC000895
Perfit MR, Fornari DJ (1983) Geochemical studies of abyssal lavas recovered by DSRV ALVIN from Eastern Galapagos Rift, Inca Transform, and Ecuador Rift. J Geophys Res 88:10530–10550
Pier JG, Podosek FA, Luhr JF, Brannon JC, Aranda-Gomez JJ (1989) Spinel-lherzolite-bearing quaternary volcanic centers in San Luis Potosi, Mexico, 2 Sr and Nd isotopic systematics. J Geophys Res B94:7941–7951
Plank T, Langmuir C (1998) The chemical composition of subducting sediment and its consequence for the crust and mantle. Chem Geol 145:325–394
Plank T, Langmuir CH (1988) An evaluation of the global variations in the major element chemistry of arc basalts. Earth Planet Sci Lett 90:349–370
Plank T, Langmuir CH (1993) Tracing trace elements from sediment input to volcanic output at subduction zones. Nature 362:739–742
Putirka K, Johnson M, Kinzler R, Longhi J, Walker D (1996) Thermobarometry of mafic igneous rocks based on clinopyroxene-liquid equilibria, 0–30 kb. Contrib Mineral Petrol 123:92–108
Putirka K, Mikaelian H, Ryerson FJ, Shaw H (2003) New clinopyroxene-liquid thermobarometers for mafic evolved and volatile-bearing lava compositions, with applications to lavas from Tibet and the Snake River Plain. Am Mineral 88:1542–1554
Putrika K (1999) CPX + Liquid equilibria. Contrib Mineral Petrol 135:151–163
Ranero CR, Morgan JP, McIntosh K, Reichert C (2003) Bending-related faulting and mantle serpentinization at the Middle America trench. Nature 425:367–373
Roeder PL, Campbell JH, Jamieson HE (1979) A re-evaluation of the olivine-spinel geothermometer. Contrib Mineral Petrol 68:325–334
Ryan J, Morris J, Bebout G, Leeman B (1996) Describing chemical fluxes in subduction zones: insights from "Depth = Profiling" Studies of arc and forearc rocks. In: Bebout G, Scholl DW, Kirby SH, Platt JP (eds) Subduction: top to bottom, Geophysical Monograph 96. AGU, Washington DC, pp 263–268
Rüpke LH, Phipps-Morgan J, Hort M, Connolly JAD (2004) Serpentine and the subduction zone water cycle. Earth Planet Sci Lett 223:17–34
Schmidt MW, Poli S (1998) Experimentally based water budgets for dehydrating slabs and consequences for arc magma generation. Earth Planet Sci Lett 163:361–379
Stern RJ, Fouch MJ, Klemperer S (2003) An overview of the Izu-Bonin-Mariana subduction factory. In: Eiler J, Hirschmann M (eds) Inside the subduction factory, vol 138. AGU Monograph, Washington DC, pp 175–222
Stern RJ, Jackson MC, Fryer P, Ito E (1993) O, Sr, Nd, and Pb isotopic composition of the Kasuga cross-chain in the Mariana Arc: a new perspective on the K-H relationship. Earth Planet Sci Lett 119:459–475
Tamura Y, Tatsumi Y, Zhaob D, Kidoa Y, Shukunoa H (2002) Hot fingers in the mantle wedge: new insights into magma genesis in subduction zones. Earth Planet Sci Lett 197:105–116
Tatsumi Y (2003) Some constraints on arc magma genesis. In: Eiler J (ed) Inside the subduction factory, vol 138. American Geophysical Union, Geophysical Monograph, Washington DC, pp 277–292
Tatsumi Y, Murasaki M, Nohda S (1992) Across-arc variation of lava chemistry in the Izu-Bonin Arc: identification of subduction components. J Volcanol Geotherm Res (49):179–190
Taylor RN, Nesbitt RW (1998) Isotopic characteristics of subduction fluids in an intra-oceanic setting, Izu-Bonin Arc, Japan. Earth Planet Sci Lett 164:79–98
Vervoort JD, Patchett PJ, Blichert-Toft J, Albarede F (1999) Relationships between Lu–Hf and Sm–Nd isotopic systems in the global sedimentary system. Earth Planet Sci Lett 168: 79–99
Vervoort JD, Patchett PJ, Söderlund U, Baker M (2004) Isotopic composition of Yb and the determination of Lu concentrations and Lu/Hf ratios by isotope dilution using MC-ICPMS. Geochem Geophys Geosyst 5(11). DOI 10.1029/2004GC000721
Wagner TP, Donnelly-Nolan JM, Grove TL (1995) Evidence of hydrous differentiation and crystal accumulation in the low-MgO, high-Al2O3 basalt from Medicine Lake volcano, California. Contrib Mineral Petrol 121:201–216
Woodhead J, Eggins S, Gamble J (1993) High field strength and transition element systematics in island arc and back-arc basin basalts; evidence for multi-phase melt extraction and a depleted mantle wedge. Earth Planet Sci Lett 114:491–504
Woodhead JD (1989) Geochemistry of the Mariana arc (western Pacific): source compositions and processes. Chem Geol 76:1–24
Woodhead JD, Eggins SM, Johnson RW (1998) Magma genesis in the New Britain island arc: further insights into melting and mass transfer processes. J Petrol 39:1041–1068
Woodhead JD, Fraser DG (1985) Pb, Sr, and 10Be isotopic studies of volcanic rocks from the Northern Mariana Islands. Implications for magma genesis and crustal recycling in the Western Pacific. Geochim Cosmochim Acta 49:1925–1930
Woodhead JD, Hergt JM, Davidson JP, Eggins SM (2001) Hafnium isotope evidence for 'conservative' element mobility during subduction zone processes. Earth Planet Sci Lett 192:331–346
Woodhead JD, Johnson RW (1993) Isotopic and trace-element profiles across the New Britain island arc, Papua New Guinea. Contrib Mineral Petrol 113:479–491
Yamasaki T, Seno T (2003) Double seismic zone and dehyration embrittlement of the subducting slab. J Geophys Res 108(B4). DOI 10.1029/2002JB001918, 002003